AEDC-TR-69-4

INVESTIGATION OF TWO TYPES OF ALARR HIGH ALTITUDE AIR SAMPLING PROBES IN SUPERSONIC LOW DENSITY AIRSTREAMS (PROJECT VELA-SURFACE)

D. W. Hill, C. E. Pinion, and D. K. Smith

ARO, Inc.

April 1969

AEROSPACE ENVIRONMENTAL FACILITY
ARNOLD ENGINEERING DEVELOPMENT CENTER
AIR FORCE SYSTEMS COMMAND
ARNOLD AIR FORCE STATION, TENNESSEE

NOTICES

When U. S. Government drawings specifications, or other data are used for any purpose other than a definitely related Government procurement operation, the Government thereby incurs no responsibility nor any obligation whatsoever, and the fact that the Government may have formulated, furnished, or in any way supplied the said drawings, specifications, or other data, is not to be regarded by implication or otherwise, or in any manner licensing the holder or any other person or corporation, or conveying any rights or permission to manufacture, use, or sell any patented invention that may in any way be related thereto.

Qualified users may obtain copies of this report from the Defense Documentation Center.

References to named commercial products in this report are not to be considered in any sense as an endorsement of the product by the United States Air Force or the Government.

INVESTIGATION OF TWO TYPES OF ALARR HIGH ALTITUDE AIR SAMPLING PROBES IN SUPERSONIC LOW DENSITY AIRSTREAMS (PROJECT VELA-SURFACE)

D. W. Hill, C. E. Pinion, and D. K. Smith
ARO, Inc.

FOREWORD

The work reported herein was performed for the Air Force Tactical Air Command (AFTAC), under System 921A, Project 9087 (Project VELA-SURFACE).

The test articles were supplied by Air Force Special Weapons Center to ARO, Inc., at the Arnold Engineering Development Center (AEDC).

The test results were obtained by ARO, Inc. (a subsidiary of Sverdrup & Parcel and Associates, Inc.), contract operator of AEDC, AFSC, Arnold Air Force Station, Tennessee, under Contract F40600-69-C-0001. The tests were conducted intermittently from October 19, 1966, to October 25, 1967, under ARO Project No. ST0611, and the manuscript was submitted for publication on November 25, 1968.

Information in this report is embargoed under the Department of State International Traffic in Arms Regulations. This report may be released to foreign governments by departments or agencies of the U. S. Government subject to approval of the Air Force Tactical Air Command (TD-6D), or higher authority within the Department of the Air Force. Private individuals or firms require a Department of State export license.

This technical report has been reviewed and is approved.

Paul L. Landry
Major, USAF
AF Representative, AEF
Directorate of Test

Roy R. Croy, Jr.
Colonel, USAF
Director of Test

ABSTRACT

Experimental investigations were made to determine aerodynamic performance of high altitude air sampling probes. Three flowthrough-type probes and a probe with a liquid-nitrogen-cooled charcoal pump were tested at pressure altitudes from 160,000 to 260,000 ft in airflows ranging from Mach number 1.8 to 3.5. The investigations indicate that the boundary layer begins to merge in the flowthrough-type supersonic diffusers below a Reynolds number per foot of 2×10^4. The charcoal pump probe indicated that there is a 0.2- to 5.0-scf transition in pumping between Reynolds numbers per foot of 1.5×10^2 and 1.4×10^4. Further investigations were made to determine the velocity attained by micron-sized particles which were generated in Mach number 3.5 low density airstreams. The results indicate the gas density was too rarefied to accelerate the particles to the free-stream velocity.

CONTENTS

ILLUSTRATIONS

APPENDIX

NOMENCLATURE

A	Area
a	Sonic velocity
C_D	Coefficient of drag
D	Drag, diameter of tube
d	Diameter of particle

K	Rate of specific heats
M	Mach number
m	Mass
P	Pressure
S	Molecular speed ratio
T	Temperature
t	Time
u	Velocity
X	Distance
Y	Distance
γ	$\frac{P_0 C_D}{\rho_p d}$
δ	Standoff distance of bow shock
η	Efficiency
ρ	Density

SUFFIXES

0	Stagnation conditions
2	Conditions behind normal shock
g	Gas
i	Initial conditions
p	Particle
∞	Free stream

PREFIXES

'	Conditions behind normal shock
*	Sonic conditions

SECTION I
INTRODUCTION

The Air Launch Air Recovery Rocket (ALARR) Program includes several types of payloads designed to remove particulate matter from the upper atmosphere. Two types are: a flowthrough probe in which the flow enters the diffuser, passes through a filter, and then is exhausted out of the payload, and a charcoal cryoadsorption probe which adsorbs the incoming air into a liquid-nitrogen-cooled charcoal bed. The flowthrough-type probe is flown at altitudes from 100,000 to 200,000 ft and the cryoadsorption probe from 160,000 to 300,000 ft.

Wind tunnel testing of the probes was necessary to simulate the flight conditions and enable prediction of the amount of the air entering the probes and their performance.

The tests were conducted in the Aerospace Research Chamber 8V (ARC 8V) (Fig. 1), which was connected to the Mark I refrigeration system to make use of the 8-kw gaseous-helium refrigeration capacity for increased cryopumping capability at the lower altitudes. A Mach number 2, low density contoured nozzle was used in the chamber to provide uniform test cores for the lower altitude tests. This nozzle was used interchangeably through the test regime with a liquid-nitrogen-cooled Mach number 3 nozzle. The working fluid for the tests was nitrogen gas.

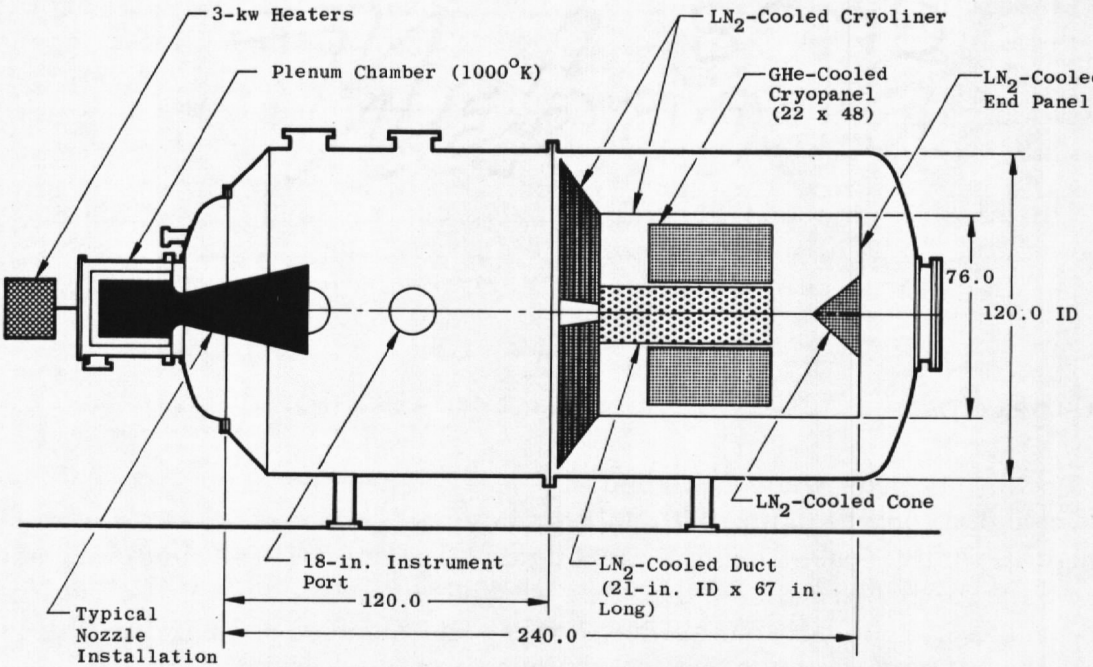

Fig. 1 Aerospace Research Chamber (8V)

The experimental investigation included five test chamber entries:

Entry	Payload Configuration	Conditions
1	a. Air Force Institute of Technology (AFIT) spiked b. AFIT unspiked	Mach number 2 Altitude, 160,000 ft 210,000 ft
2	No payload, particle generation and counting	Mach number 3.5 Altitude, 275,000 ft
3	a. Varian liquid-nitrogen-cooled charcoal	a. Mach number 1.8 to 3.5 Altitude, 160,000 ft 275,000 ft
	b. AFIT unspiked inlet	b. Mach number 3.5 Altitude, 230,000 ft 275,000 ft
4	Varian	Mach number 1.9 to 3.5 Altitude, 160,000 ft 250,000 ft
5	Modified AFIT	Mach number 1.9 to 3.5 Altitude, 160,000 ft 250,000 ft

SECTION II
DESCRIPTION OF TEST ARTICLES

The ALARR payloads were all of ogive shape, each approximately 3 ft long and 1.5 ft at the largest diameter, with the inlets being about 5 in. in diameter. The dimensions of each payload are given in Figs. 2 and 3.

2.1 AFIT PAYLOADS

These payloads were designed at AFIT, hence the name. They are flowthrough-type air sampling probes where the ingested gases enter through the inlet, pass through a diffusing section, a filter medium, and turning vanes and are then exhausted around the periphery of the payload near its base. The filter material covers the exhaust area immediately inside the turning vanes and is sandwiched for support between a 0.125-in. grid and a No. 10 copper mesh screen.

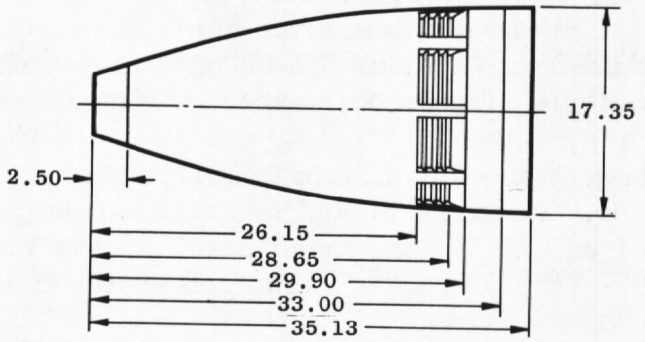

All Dimensions in Inches

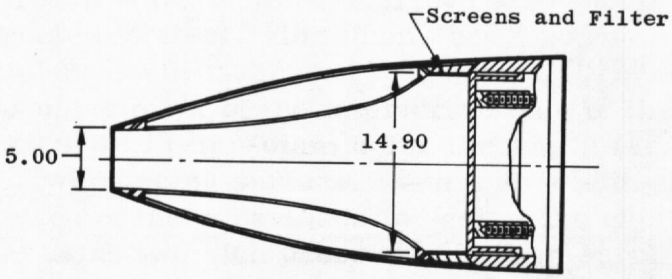

Fig. 2 Details and Dimensions of Unspiked AFIT Payload

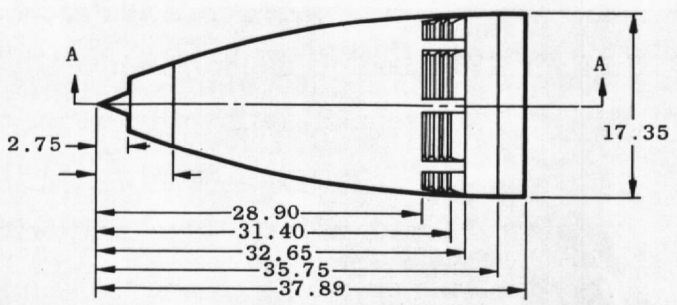

All Dimensions in Inches

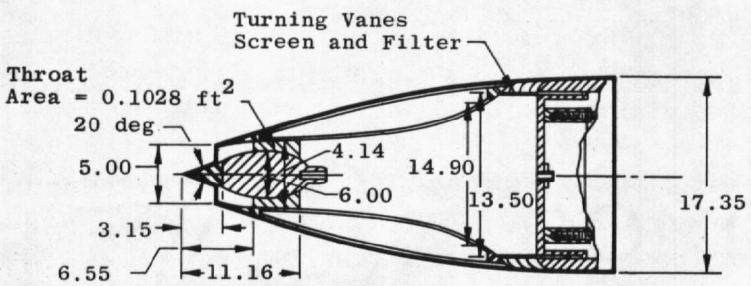

Fig. 3 Details and Dimensions of Spiked AFIT Payload

2.2 UNSPIKED AFIT PAYLOAD

The external shell and internal diffuser are constructed of fiber glass, whereas the inlet section, exhaust section, and base are of aluminum and steel. The diffuser section (Fig. 2) diverges from the 5-in. -diam inlet to 14. 9 in. at the exhaust area.

2.3 SPIKED AFIT PAYLOAD

This payload (Fig. 3) is essentially the same as the unspiked AFIT payload but with a steel spike in the inlet and a slightly different contour for the diffuser immediately inside the inlet.

2.4 MODIFIED AFIT

This payload (Fig. 4) is a modification of the unspiked AFIT payload with a redesigned inlet lip, diffuser, and exhaust area.

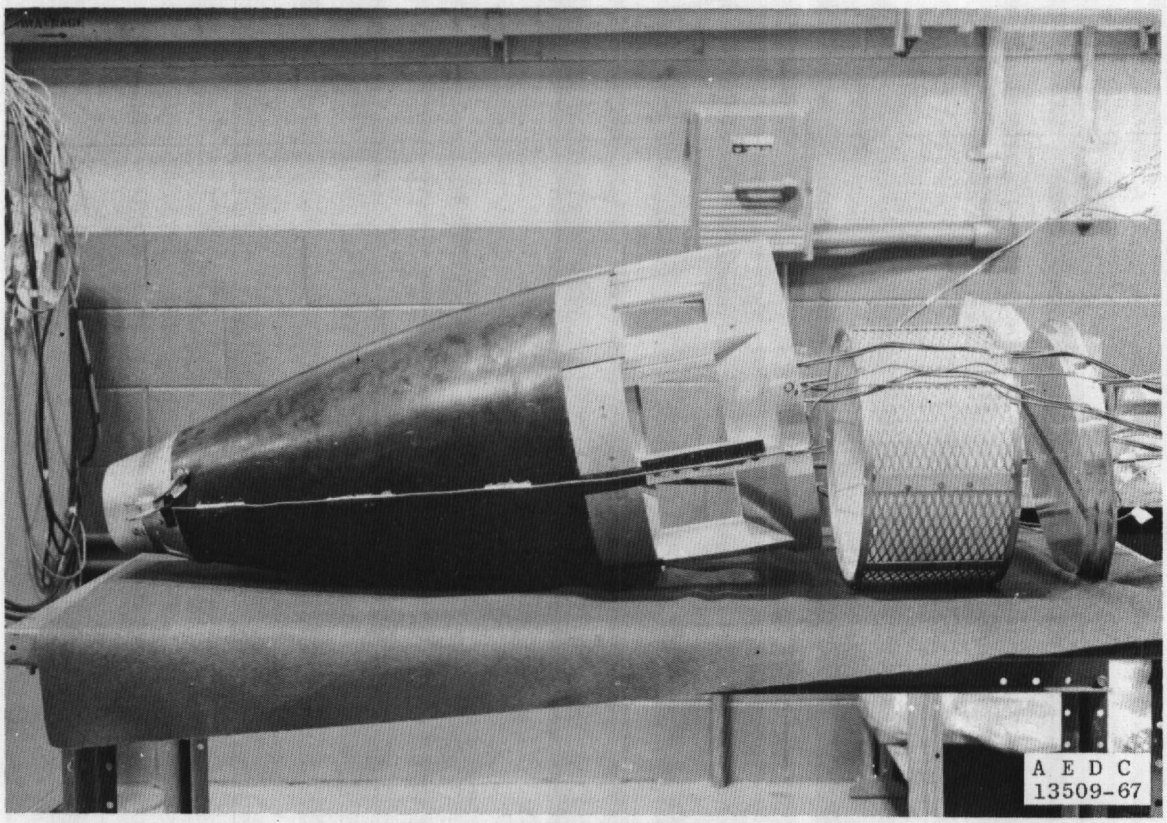

Fig. 4 Modified AFIT with Filter Basket

The inlet lip was redesigned to decrease the angle of divergence so the gas passing over the outer surface of the payload would not be turned so abruptly at the inlet. The inlet diameter remained unchanged, but this modification slightly increased the overall length of the payload.

The diffuser, constructed of aluminum, consists of a cylindrical section beginning at the inlet and a double conical divergent section ending at the exhaust area. The exhaust area of this payload has been doubled over the previous designs.

2.5 VARIAN PAYLOADS

These payloads (Fig. 5) were designed and built by Varian Associates and are constructed of steel, aluminum, and charcoal. The gas flowing into these payloads is cryoadsorbed by a liquid-nitrogen-cooled charcoal pump which occupies most of the interior volume of the payload. The charcoal pump has 48, 1-in.-diam holes through its length, giving approximately 264 $in.^2$ of pumping surface. There is a leak-tight butterfly valve in the inlet of each of these payloads to seal in the captured gases. It is piston operated using two high pressure nitrogen supplies. The valve is normally held closed by 600-psi pressure and is opened by an overriding 1400-psi pressure. The payload as installed in the ARC 8V is shown in Fig. 6.

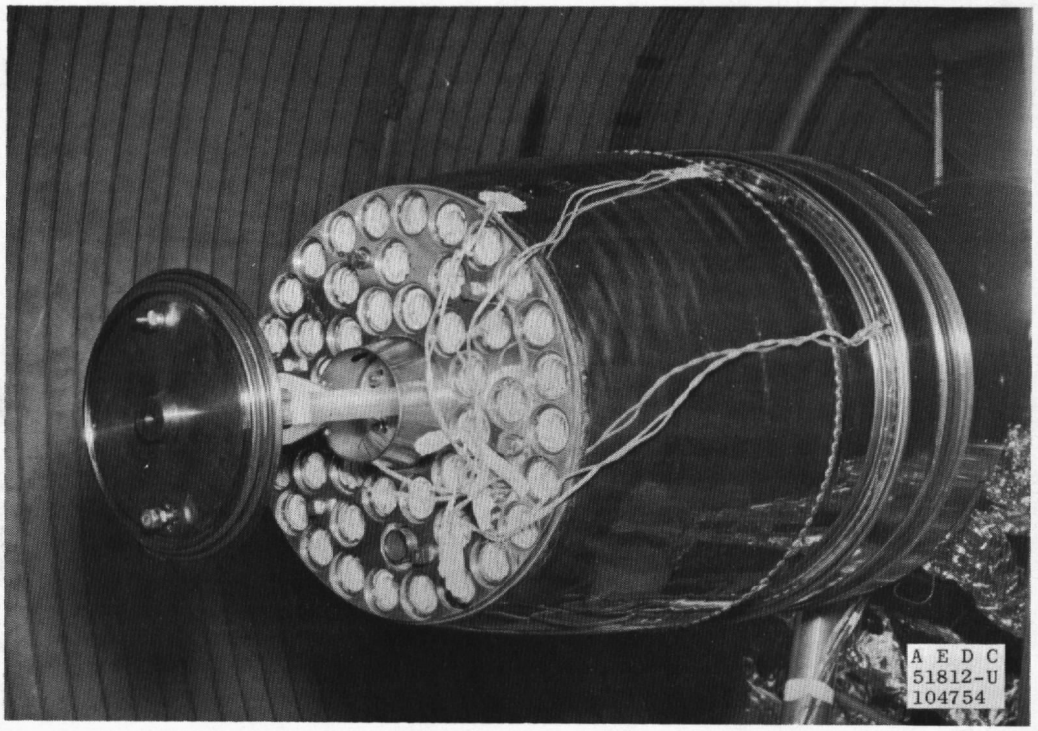

Fig. 5 Varian Payload, Configuration 1

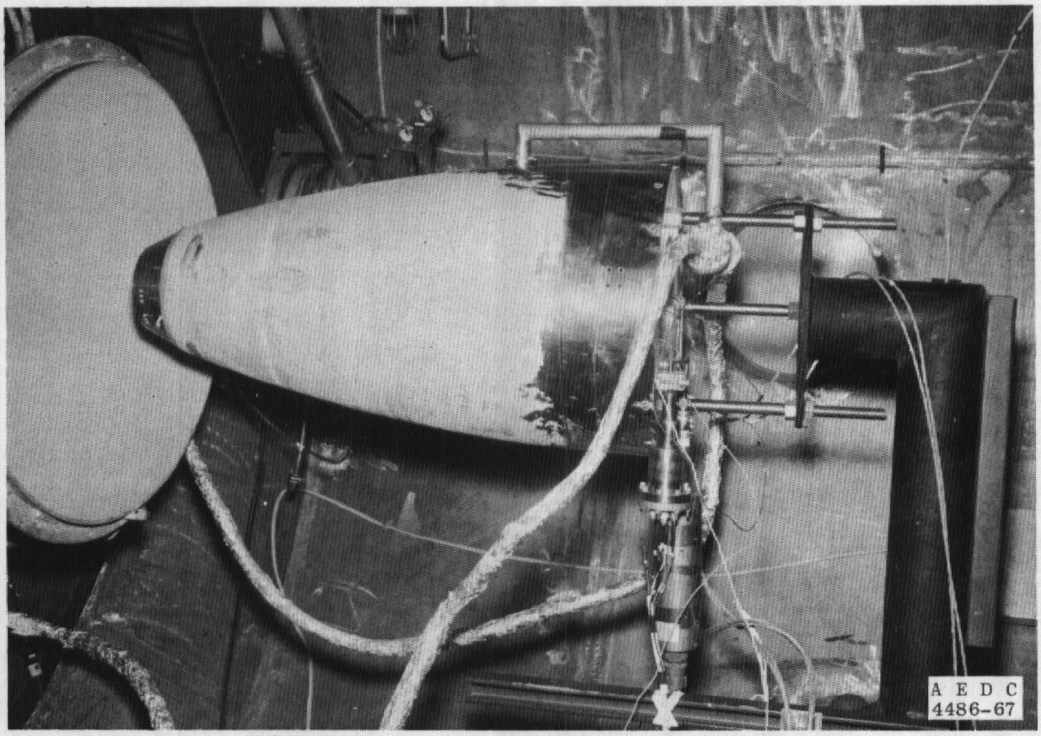

Fig. 6 Varian Payload and Mach Number 3 Nozzle in ARC 8V

In configuration 1 of this payload, each of the holes in the charcoal cryopump is lined with the filter material which is held in place by springs. Configuration 2 differs only in that, in addition, there is a disk of filter material covering the entire frontal area of the charcoal cryopump, resulting in double filtering of the ingested gas.

SECTION III
DESCRIPTION OF TEST FACILITY

The tests were conducted in the ARC 8V, a 10-ft-diam by 20-ft-long stainless steel vacuum chamber used primarily for low density aerodynamic testing in the transition and free-molecular flow regimes. For these tests, two interchangeable nozzles were employed which provide nominal Mach number 2 and 3 gas flows at their exits. The working gas, in this case nitrogen, is pumped by 120 ft^2 of gaseous-helium (20°K)-cooled cryopanels arranged in a radial array in the downstream half of the chamber. Pressure altitudes can be simulated from 150,000 to 320,000 ft, depending on which of the nozzles is used.

The Mach number 3 nozzle is a conical, aluminum nozzle having a liquid-nitrogen-cooled throat and divergent section to reduce boundary-layer thickness. The Mach number 2 nozzle, used for the lower simulated altitudes, is an uncooled, contoured fiber glass nozzle. A typical nozzle installation for aerodynamic testing in the ARC 8V is shown in Fig. 1.

The payloads were mounted on a support mechanism which supported the payloads at the rear. This mechanism could be pivoted in a horizontal plane about a vertical axis passing through the center of the payload inlet to simulate various angles of attack from 0 to 20 deg.

3.1 VARIAN (CONFIGURATIONS 1 AND 2)

To cool the charcoal cryopump in the Varian payload, it was connected to the existing liquid-nitrogen supply to the ARC 8V chamber. The charcoal was warmed by flowing heated nitrogen gas through the liquid-nitrogen shroud surrounding the aft end of the charcoal. The nitrogen was supplied from compressed gas cylinders and passed through a coil of 0.5-in.-diam copper tubing which was heated resistively by passing a large electrical current through the coil. The current was furnished from several high current transformers, each controlled by a variable rheostat.

The inlet valve on the Varian payload was operated from outside the chamber using two bottles of compressed nitrogen gas, one regulated to 600 psi to keep the valve closed and the other regulated to 1400 psi to override the 600 psi and open the valve. Two normally closed solenoid valves were used in the 1400-psi pressure system to apply and release the pressure as required to operate the valve.

3.2 UNSPIKED AND MODIFIED AFIT

In Fig. 7 a 0.250-in.-OD horizontally traversing total pressure probe is shown schematically in the exhaust section of the Unspiked AFIT payload. This probe was also used with the Modified AFIT payload. The probe was operated manually from outside the chamber.

With the modified AFIT payload, a sliding sleeve was mounted close around the aft end of the payload (Fig. 8) to decrease the exhaust area by one-half when the sleeve was in the forward position. Normally, the sleeve was fully retracted to allow for the full exhaust opening. The sleeve was positioned by an air-actuated piston controlled from outside the chamber.

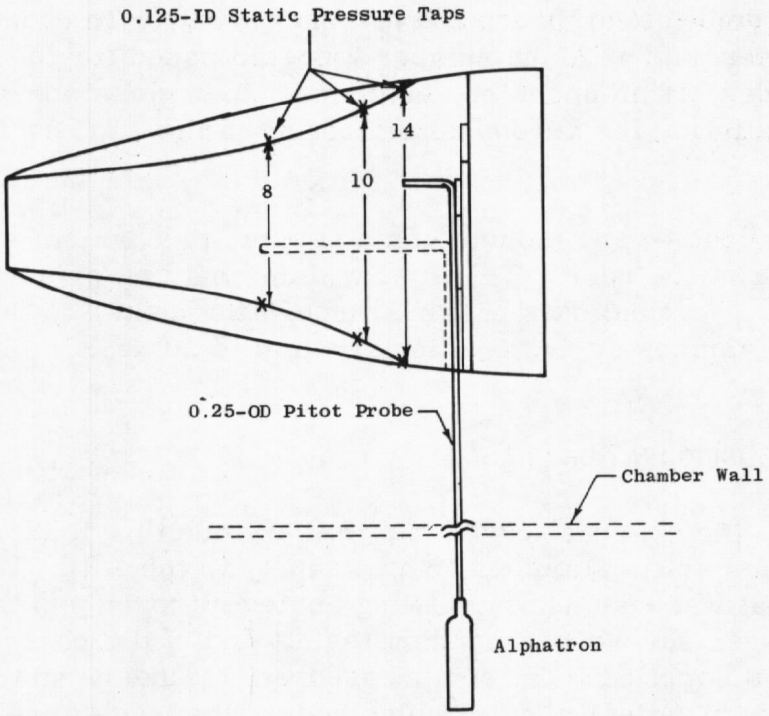

Fig. 7 Unspiked AFIT Payload with Instrumentation Locations

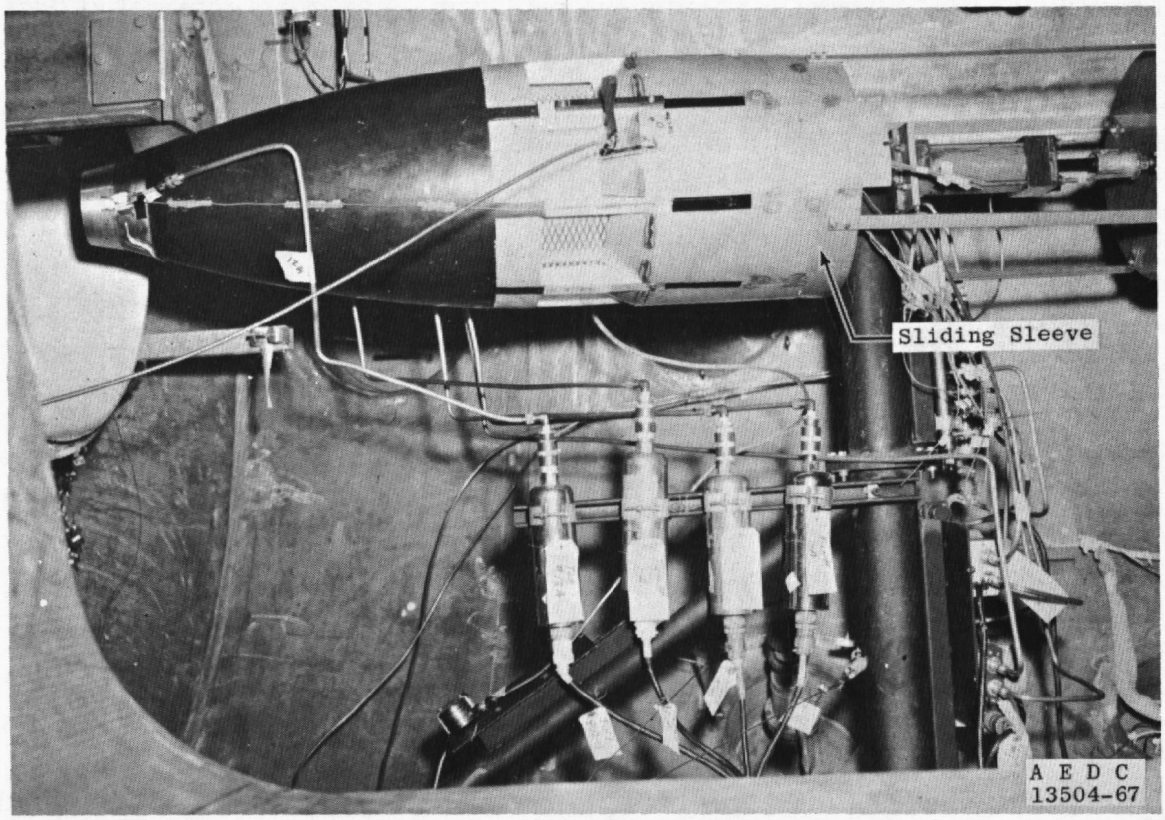

Fig. 8 Modified AFIT in ARC 8V

SECTION IV
TEST INSTRUMENTATION

The nozzle plenum pressure for both the Mach number 2 and 3 nozzles was measured with an Alphatron® pressure gage. A nude ionization gage was mounted in the test section of the chamber to monitor the chamber background pressure below 10^{-3} torr before testing.

4.1 UNSPIKED AFIT PAYLOAD

Static pressure data in this payload were taken with one Alphatron connected to each of three pairs of diametrically opposed static pressure taps located in the diffuser wall at diffuser diameters of 8, 10, and 14 in. A horizontally traversing total pressure probe connected to an Alphatron was used to measure total pressure between the static pressure taps at the 8-in. diffuser diameter, and another similar probe was used to measure the total pressure between the static pressure taps located at the 14-in. diffuser diameter as indicated in Fig. 7.

An Alphatron on the Mach number 3 nozzle skirt measured nozzle static pressure, and an Alphatron in the chamber test section was used to monitor pressures during test runs.

A radio frequency oscillator with the antenna placed about the payload inlets was used to excite the nitrogen gas so the flow could be observed visually and photographed.

4.2 MODIFIED AFIT PAYLOAD

During test runs 1 through 12, static pressures were measured with Alphatrons and Baratrons®, whereas the two total pressures were measured with a Lion® gage and a Baratron. Chamber static pressure near the test section was measured with an Alphatron during test runs 13 through 28, but on runs 29 through 33 this Alphatron was used to obtain Mach number 3 nozzle static pressure.

4.3 VARIAN PAYLOAD (CONFIGURATIONS 1 AND 2)

The pressure inside the payload was measured through a small diameter tube passing completely through the charcoal to the rear of the payload where an Alphatron was connected.

SECTION V
PROCEDURE

5.1 UNSPIKED AFIT

A total of 19 test runs were made on the unspiked AFIT payload in the ARC 8V under the following conditions:

Without Filter

Altitude, Z, ft	Angle of Attack, α, deg	Diffuser Diameter, in.
300,000	0	8 and 14
275,000	0	8 and 14
275,000	5	14
275,000	10	8 and 14
250,000	0	8 and 14
250,000	10	8 and 14

With Double Thickness of 0.25 Basic Weight Filter

Altitude, Z, ft	Angle of Attack, α, deg	Diffuser Diameter, in.
250,000	0	8 and 14
250,000	10	8 and 14
240,000	0	8 and 14
240,000	10	8 and 14

Average static pressure measurements were made at the wall of the diffuser at diffuser diameters of 8, 10, and 14 in. Total pressure measurements were made with a horizontally traversing probe at 1-in. intervals across the 14-in. diffuser diameter and at 0.5-in. intervals across the 8-in. diffuser diameter. Pressure readings were recorded only after all pressure gages had stabilized.

5.2 MODIFIED AFIT

A total of 33 test runs were made on the modified AFIT payload under the following conditions:

Run No.	Mach Number, M	Altitude, Z, ft	Angle of Attack, α, deg	Filter Weight, W	Exit Area Fraction, A
1	2	190,000	0	1	1
2	2	190,000	10	1	1
3	2	190,000	15	1	1
4	2	190,000	0	1	0.5
5	2	175,000	0	1	0.5
6	2	175,000	0	1	1
7	2	175,000	10	1	1
8	2	175,000	15	1	1
9	2	160,000	15	1	1
10	2	160,000	10	1	1
11	2	160,000	0	1	1
12	2	160,000	0	1	0.5
13	2	210,000	0	0.5	0.5
14	2	210,000	0	0.5	1
15	2	210,000	10	0.5	1
16	2	210,000	15	0.5	1
17	2	190,000	15	0.5	1
18	2	190,000	10	0.5	1
19	2	190,000	0	0.5	1
20	2	190,000	0	0.5	0.5
21	2	175,000	0	0.5	0.5
22	2	175,000	0	0.5	1
23	2	160,000	0	0.5	1
24	2	175,000	10	0.5	1
25	2	175,000	15	0.5	1
26	2	160,000	15	0.5	1
27	2	160,000	10	0.5	1
28	2	160,000	0	0.5	0.5

Run No.	Mach Number, M	Altitude, Z, ft	Angle of Attack, α, deg	Filter Weight, W	Exit Area Fraction, A
29	3	240,000	0	0.5	0.5
30	3	250,000	0	0.5	0.5
31	3	250,000	0	0.5	1
32	3	250,000	10	0.5	1
33	3	250,000	15	0.5	1

Static pressure measurements were made internal and external to the inlet section, along the diffuser wall, and internal and external to the exhaust area. Total pressure measurements were made with a traversing pressure probe in 1.0-in. intervals across a diameter even with the front of the exhaust section and with a stationary tap on the back plate of the exhaust section near the filter. See Fig. 9 for location of pressure taps.

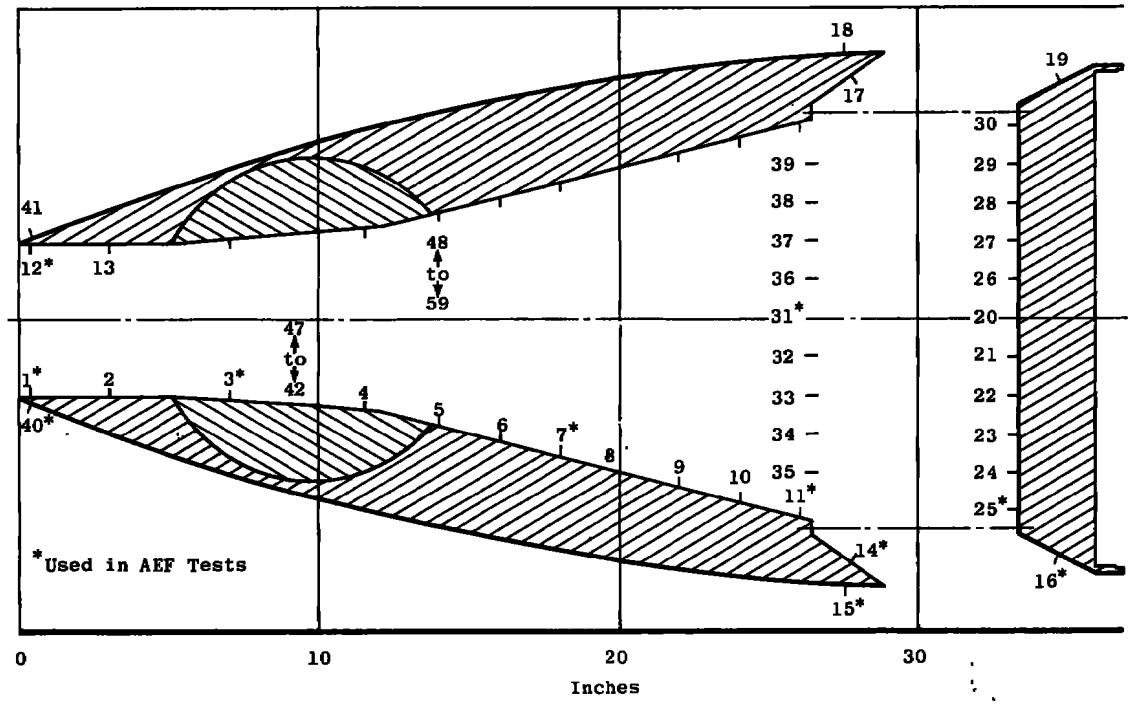

Fig. 9 Location of Pressure Taps, Modified AFIT

5.3 VARIAN TEST, CONFIGURATION 1

Before testing began, the chamber was pumped down to 10^{-8} torr, and the payload charcoal cryopump was baked out for 3 hr at 480°F with the inlet valve open. This initial bakeout was performed whenever the

charcoal had been previously exposed to the atmosphere. Air collection efficiency tests were then started and performed for the following conditions:

Mach Number	Angle of Attack, deg	T_0[1], °R	Simulated Pressure Altitude, ft	P_0[1], mm Hg
3.5	0	530	260,000	0.770
3.5	0		240,000	1.75
3.5	15		240,000	1.75
1.75	0		210,000	0.50
1.75	15		210,000	0.50
1.91	0		180,000	2.20
1.91	15		180,000	2.20
1.94	0		160,000	4.90
1.94	15		160,000	4.90

Before each test run the charcoal was cooled for approximately 6 hr with liquid nitrogen until the front temperature sensor indicated approximately -290°F; a typical cooldown curve is shown in Fig. 10. The gas flow through the nozzle was then started and allowed to stabilize. The payload inlet valve was opened and left open until the payload pressure ceased rising, indicating that the shock had moved out of the inlet. At this time the inlet valve was closed. The charcoal was heated with hot nitrogen at 450°F until the front temperature sensor indicated approximately 110°F. The hot nitrogen flow was then stopped, and the charcoal temperature was allowed to stabilize at room temperature before the payload internal pressure was recorded and the collected gas released. The warmup procedure required about a total of 12 hr; a typical warmup curve is shown in Fig. 11.

5.4 VARIAN PAYLOAD, CONFIGURATION 2

The pretest procedures for this payload were the same as for Configuration 1 with two exceptions: The charcoal was baked out for approximately 4 hr with the inlet valve open before each test run rather than only after exposure to the atmosphere, and the charcoal was activated by cooling for 8 hr rather than 6 hr.

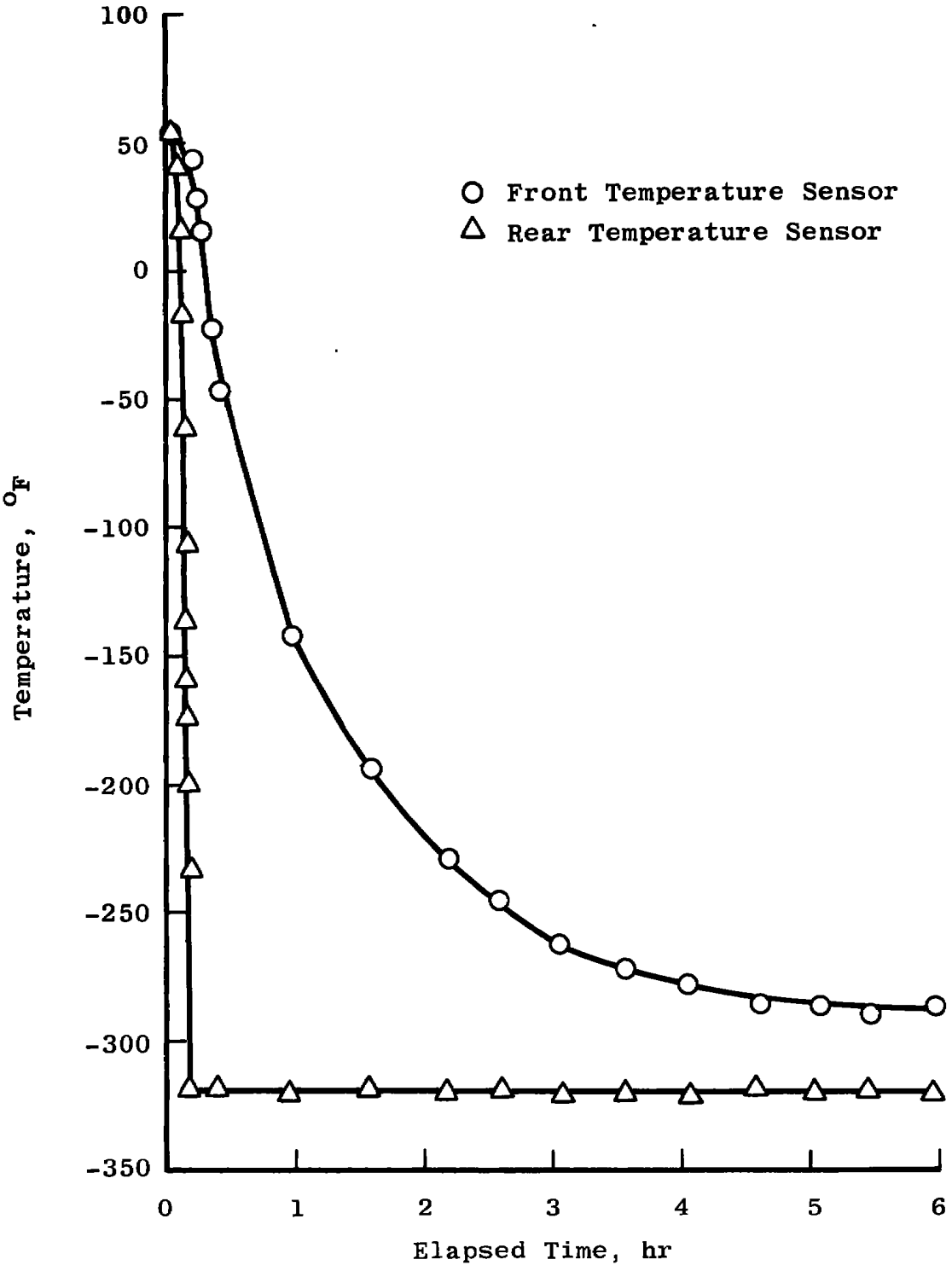

Fig. 10 Typical Cooldown Time versus Temperature, Varian Payload

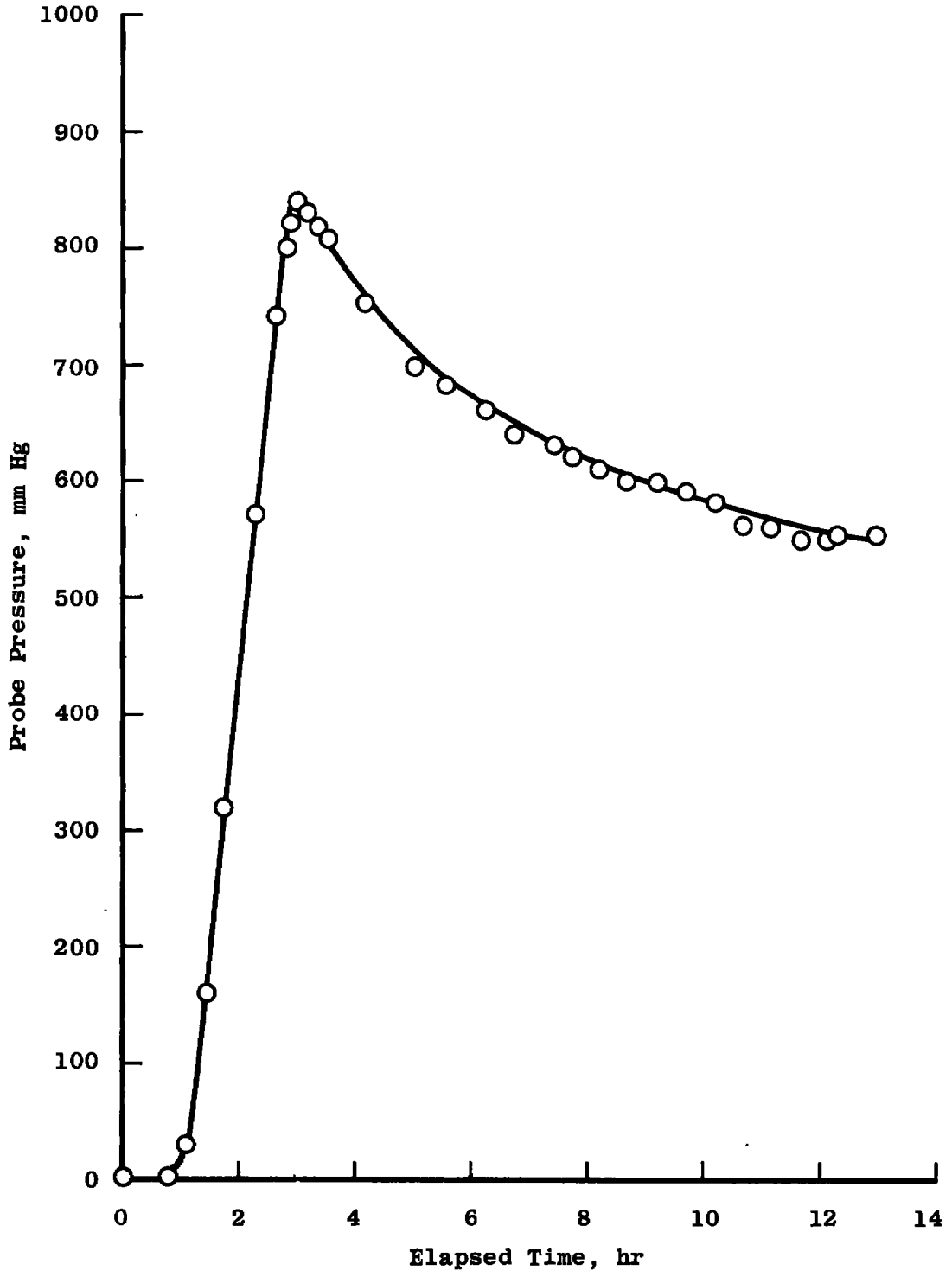

Fig. 11 Typical Warmup Time versus Pressure, Varian Payload

Air collection efficiency tests were conducted for Configuration 2 under the following conditions:

Mach Number	Angle of Attack, deg	T_0[1], °R	Simulated Pressure Altitude, ft	P_0[1], mm Hg
3.5	0	530	260,000	0.77
3.5	↓	↓	240,000	1.75
1.94	↓	↓	160,000	4.90

The posttest procedures for this configuration were the same as for Configuration 1.

To get an indication of the charcoal temperature, two platinum temperature sensors were employed, one placed near the liquid-nitrogen shroud around the aft end of the charcoal and the other placed near the fore end of the charcoal. The sensors were read out on a dual pen strip chart recorder and the system calibrated with two constant current power supplies and a digital voltmeter.

SECTION VI
RESULTS AND DISCUSSION

6.1 ALARR PAYLOADS

Figures 12 and 13 show the calibration results of the Mach number 2 and 3 low density nozzles. In the figures, free-stream Mach number, Reynolds number per foot, and altitude are plotted as functions of nozzle reservoir pressure.

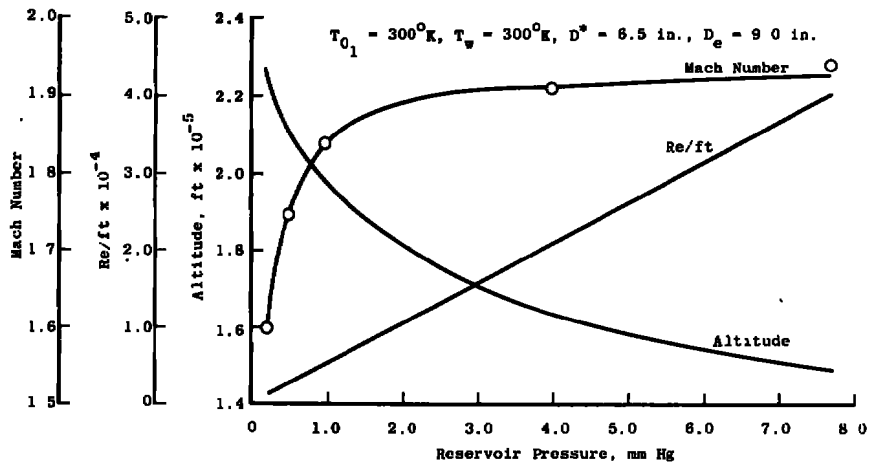

Fig. 12 Free-Stream Calibration Results of Mach Number 2 Fiber Glass Nozzle

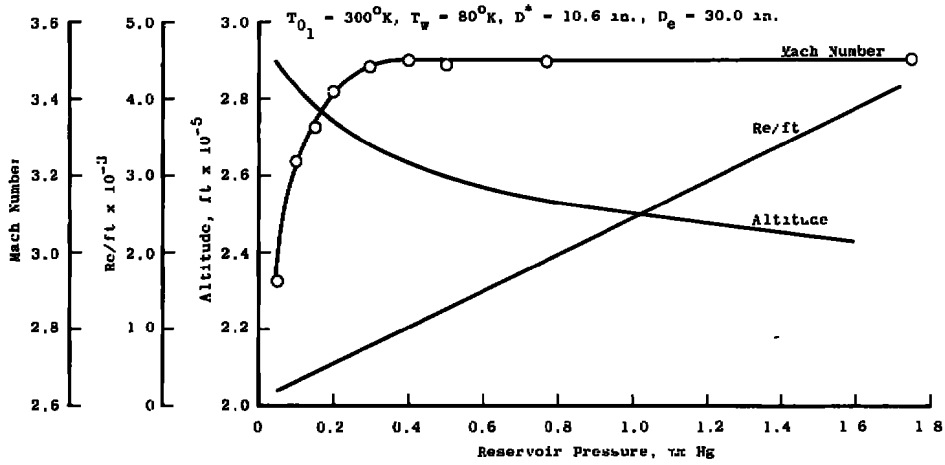

Fig. 13 Free-Stream Calibration Results of Mach Number 3 Nozzle

The tests of the unspiked and spiked AFIT payload showed from visual observation that the payloads were very altitude limited in Mach number 2 flows. The flow visualization of the spiked inlet payload showed the oblique and normal shocks attached only at 160,000-ft altitude. The unspiked AFIT inlet payload from test chamber entries 1 and 3 was found to be operational from 160,000- to 235,000-ft altitudes with a filter paper of one-half the basic weight. Figure 14 shows the total pressure survey in the 8-in. -diam diffuser section without filter paper. Since the exit area is two and one-half times greater than the inlet area, at the lower altitudes the shock is completely swallowed. The flow separates from the diffuser wall when passing through the inlet. As the altitude is increased, the boundary layer in the diffuser merges.

Figures 15, 16, and 17 show the effect with the filter paper of one-half the basic weight added to the exhaust area. The addition of the filter resulted in a more favorable pressure gradient along the diffuser wall. The pressure recovery is at a maximum, and the normal shock is attached to the inlet. Figure 18 shows no significant loss in total pressure in the payload at an angle of attack of 10 deg.

Figure 18 shows typical variations in nozzle static and Varian payload pressures with run time. With the payload valve closed, the detached inlet normal shock causes an increase in nozzle static pressure. When the valve is open, the shock is swallowed until the charcoal has reached its adsorbing limit; then, the shock begins to move out of the inlet, again causing an increase in nozzle static pressure. The payload and nozzle static pressures were used to determine the payload maximum sampling times which, by definition, correspond to the time the normal shock remains within the inlet.

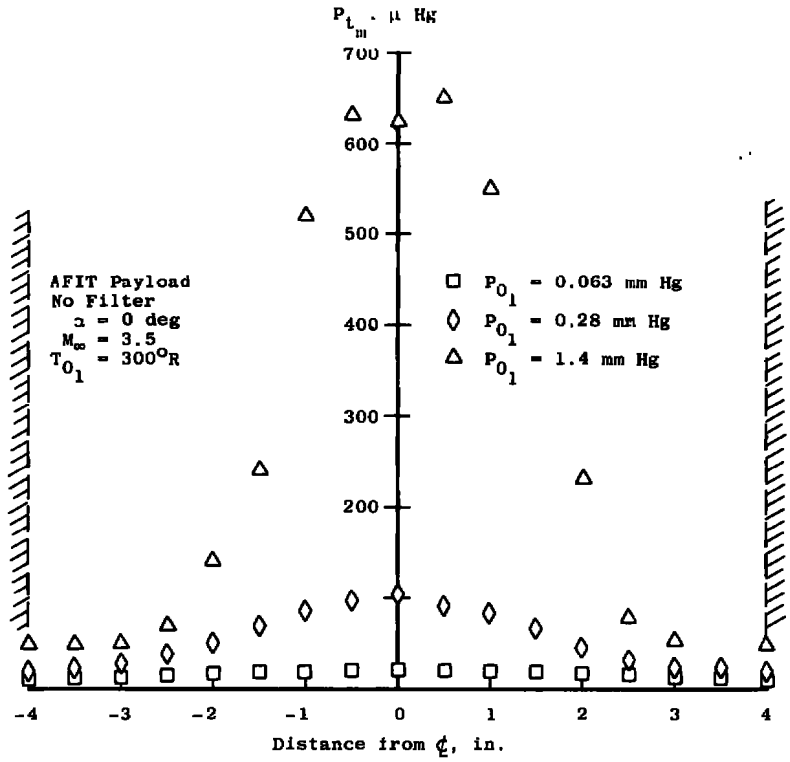

Fig. 14 Measured Total Pressure inside AFIT Payload, without Filter Paper, 8-in. Station

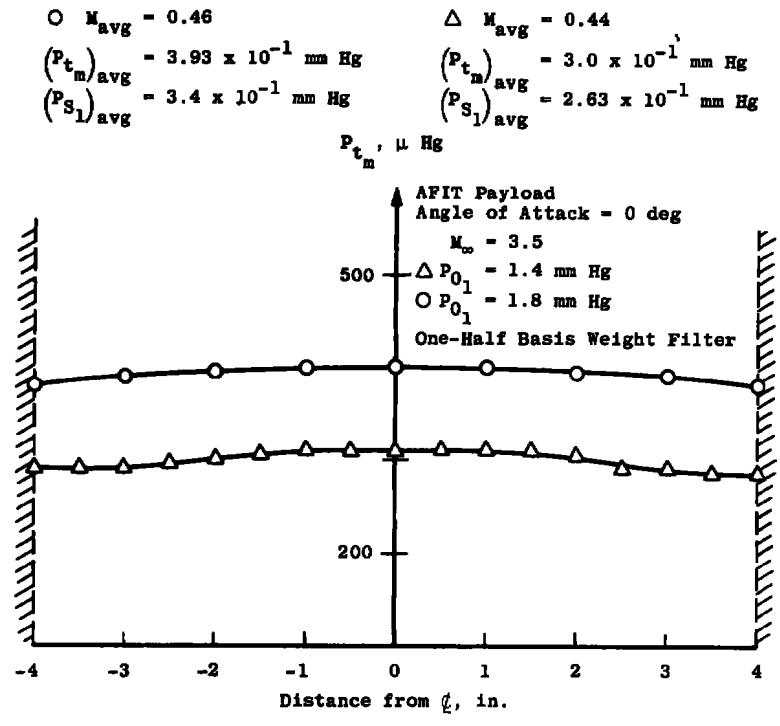

Fig. 15 Measured Total Pressure inside AFIT Payload, with Filter, 8-in. Station

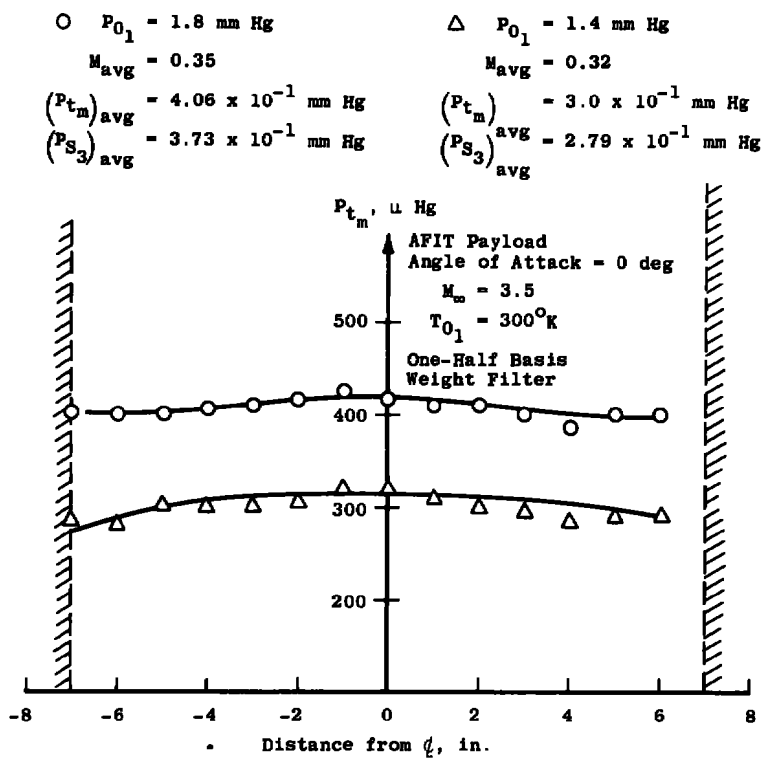

Fig. 16 Measured Total Pressure inside AFIT Payload, with Filter, 14-in. Station

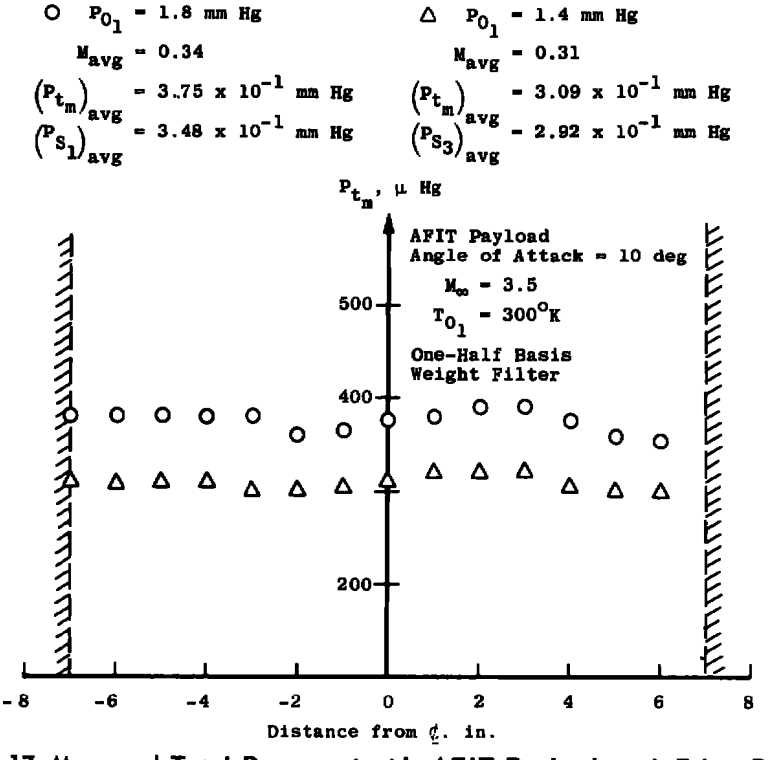

Fig. 17 Measured Total Pressure inside AFIT Payload, with Filter Paper, 8-in. Station, 10-deg Angle of Attack

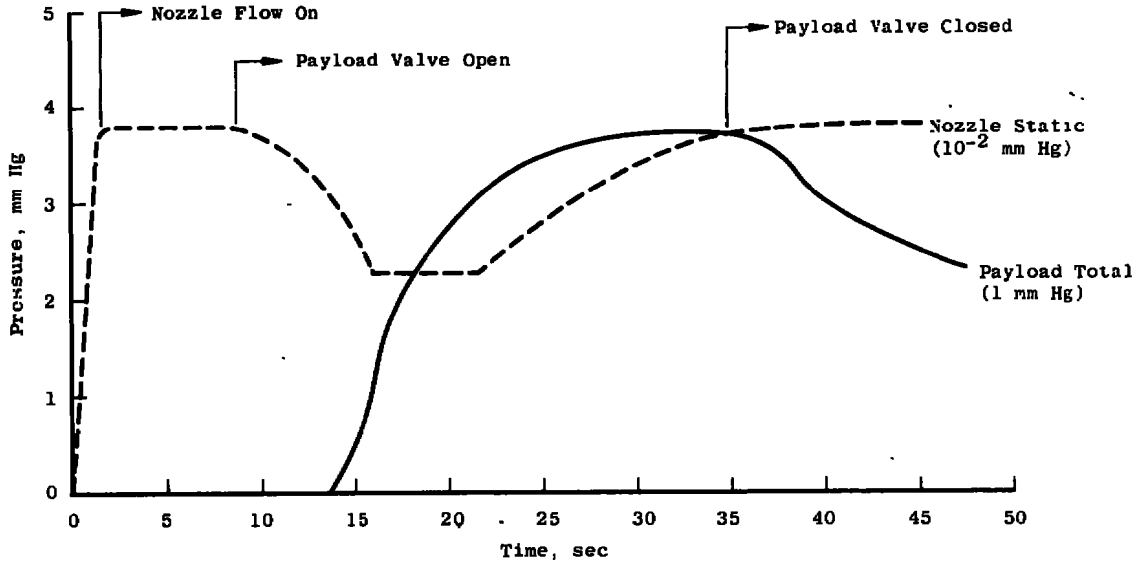

Fig. 18 Typical Pressures versus Run Time, Varian Payload

Figure 19, based on data from Ref. 1, shows the pressure drop across IPC 1478 filter paper, used in the air sampling probes, versus free-stream Reynolds number per foot. Below 6 x 10^4 Reynolds number per foot the pressure drop across the paper increases significantly with decreasing Reynolds number.

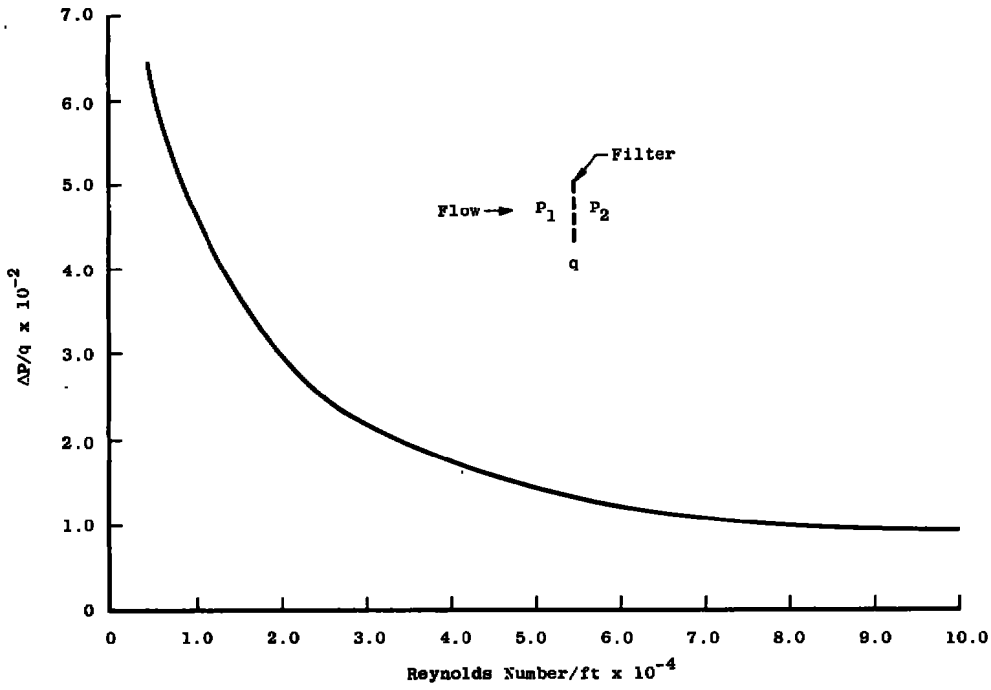

Fig. 19 Pressure Drop versus Reynolds Number for IPC 1478 Filter Paper

In Fig. 20 are plotted gas volume captured in the payload and the maximum sampling time as functions of free-stream Reynolds number per foot over Mach number (the inverse Knudsen number). The curves indicate there is a transition in the gas volume captured between Reynolds number per foot of 1.5×10^2 and 1.4×10^4. This transition is caused by the viscosity effects on the pressure drop across the filter paper. While data are in general agreement with those of Ref. 2, it is concluded that the viscous effect rather than the charcoal adsorption rate limits the amount of gas captured. This is evident when the payload valve is closed after sampling and the pressure in the payload decreases. Varian payload Configuration 2, in which a filter paper of one-half the basic weight was placed normal to the opening of the tubes, captured only one-third the gas that Configuration 1 captured for the same sampling times.

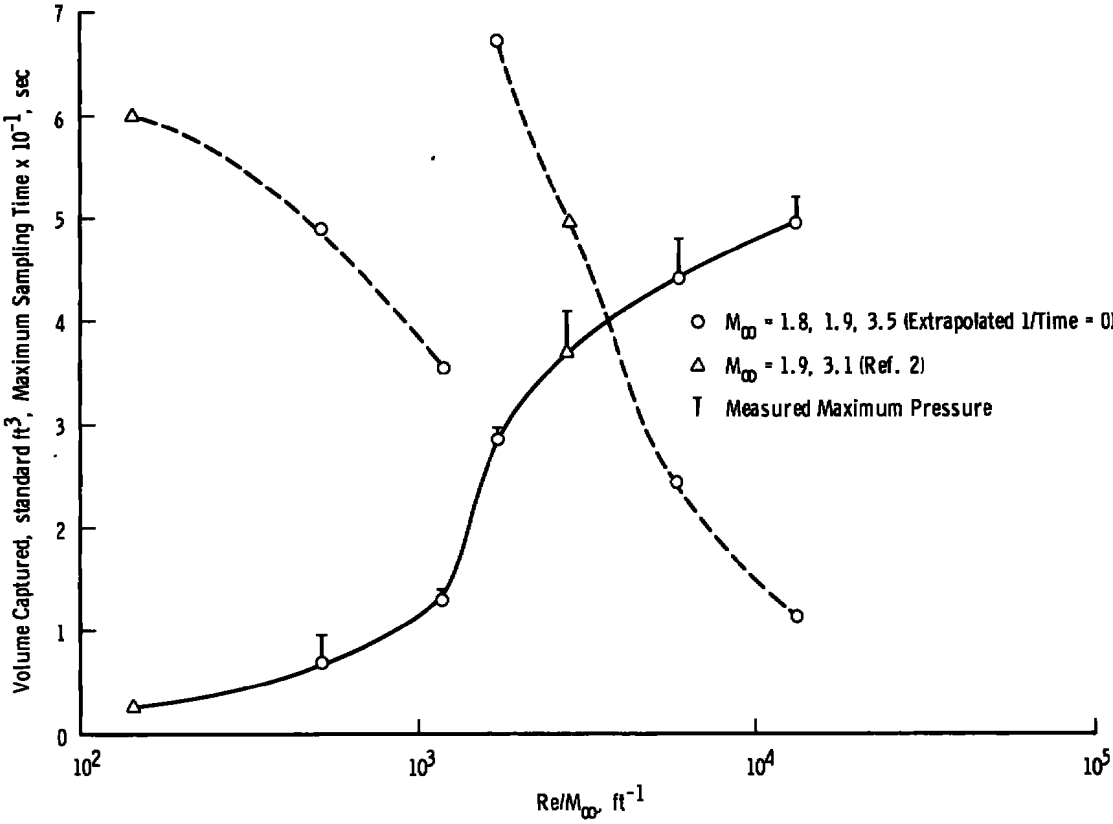

Fig. 20 Volume Captured and Sampling Time versus Re/M_∞

6.2 PARTICLE VELOCITY AND CONCENTRATION MEASUREMENTS

Since one of the original purposes of these tests was to determine the particle collection efficiency of the ALARR payloads, it was necessary to inject particles into the gas flow and attempt to determine their

velocity relative to the free-stream gas velocity. Ammonium chloride and aluminum chloride were heated and sublimed into the nozzle plenum chamber to create particles from about 0.1 to 5 or 6μ in diameter. Attempts to spray a solid in suspension through a small diameter nozzle into the plenum chamber to create small particles proved unsuccessful because of solidification of the suspension and clogging of the nozzle on encountering the low pressure in the plenum chamber.

After considering various ways of measuring particle velocity in the gas flow, it was decided a light scattering technique based on Mie's theory would be best, since it would not be necessary to place any flow-disturbing object in the particle-gas flow.

6.2.1 Single Beam Technique

The first attempt to measure particle concentration and velocity in the gas stream at the nozzle exit employed a single continuous, helium-neon polarized laser beam directed horizontally across the diameter of the Mach number 3 nozzle and several inches downstream from the nozzle exit (Fig. 21). A 7102 photomultiplier tube was mounted at the top edge of the nozzle exit looking vertically downward at the laser beam, since according to Mie's light scattering theory the maximum light is scattered at 90 deg to the incident beam. The photomultiplier slit length was oriented perpendicular to the length of the laser beam, and a lens focused the beam onto the slit. Particles passing through the laser beam in the field of view of the photomultiplier tube reflect light into the tube. The tube then feeds a signal into an oscilloscope which was adjusted so that the sweep was triggered only by signals above a certain strength. The oscilloscope traces produced by each particle passing through the laser beam in the field of view of the photomultiplier tube were photographed. Knowing the width of the laser beam and the sweep time of the oscilloscope, the velocity of the particles could be determined from the measured peak width of the traces.

6.2.2 Double Beam Technique

The measurement of particle approximate velocities was also attempted by determining the flight times between two parallel helium-neon laser beams 0.4 in. apart in a horizontal plane placed several inches downstream from the nozzle exit across the nozzle diameter. The photomultiplier, located as previously described, ideally gives a double pulse as the particle traverses these beams; the particle flight times may be determined from the separation distance and the measured pulse width. The beam separation was determined in part by considering the sweep time and response time of the oscilloscope. The pulses are then

processed electronically (shaped and gated) for counting and recording purposes. The purpose in the specific design was to establish a means for measuring the mean velocity, and ultimately, with the addition of more elaborate instrumentation, the velocity distribution by recording individual particle velocities.

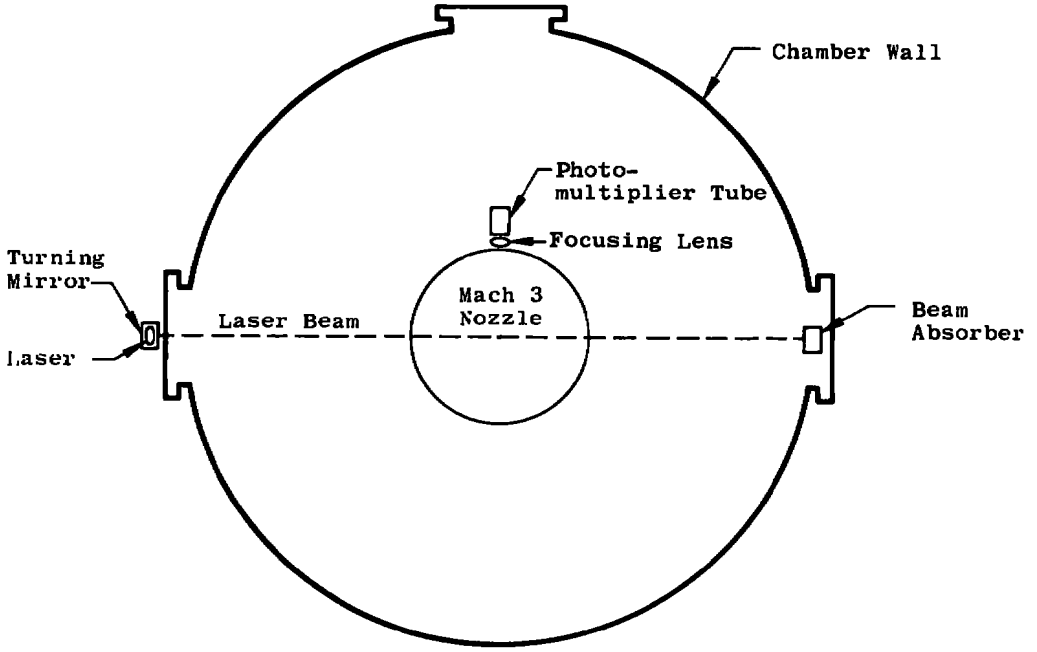

View Looking into Nozzle

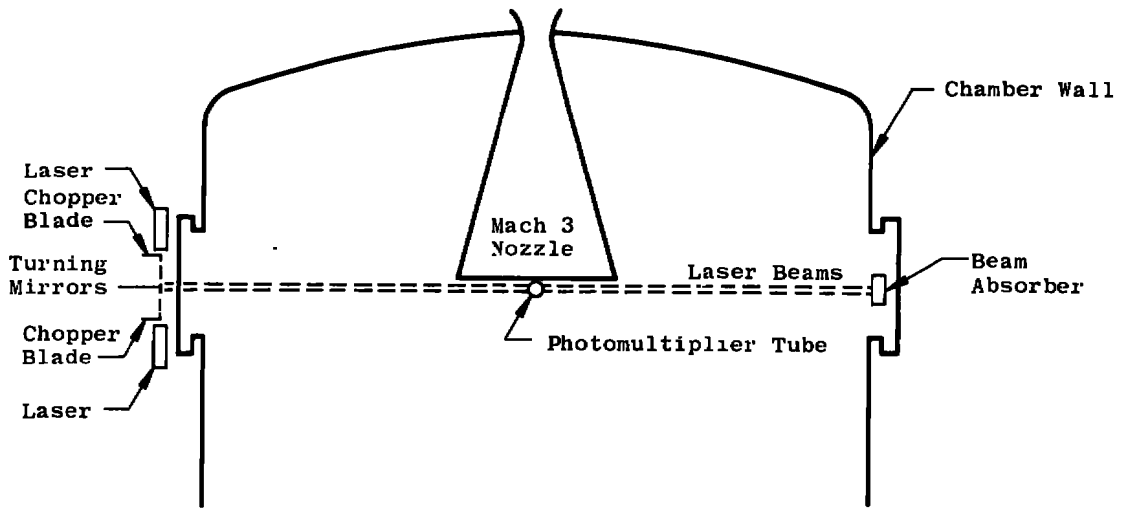

Top View

Fig. 21 Schematic of Particle Velocity Apparatus

Shown in Fig. 22 is the block diagram of the basic system. The associated timing diagram is shown in Fig. 23. The function designated Gate A1 is the duration of the scope sweep and is set at a time slightly greater than twice the maximum flight time anticipated. This time is required to assure that subsequent particles do not initiate gating functions until all previous operations are complete. Time Base B is set at a pulse width sufficient to set a lower boundary on the particle flight times. Delay time t_2 is set slightly longer than the width of Gate B1 and serves the purpose of assuring the use of doublets that only have the first pulse occurring at the time of Gate A1. The system, as designed, delays each pulse of a doublet an equal amount, and the separation of the trailing edge of these delays (t_1) is indicative of the flight time. Figure 23 also shows various situations where the existence of multiplier pulses will not be recorded.

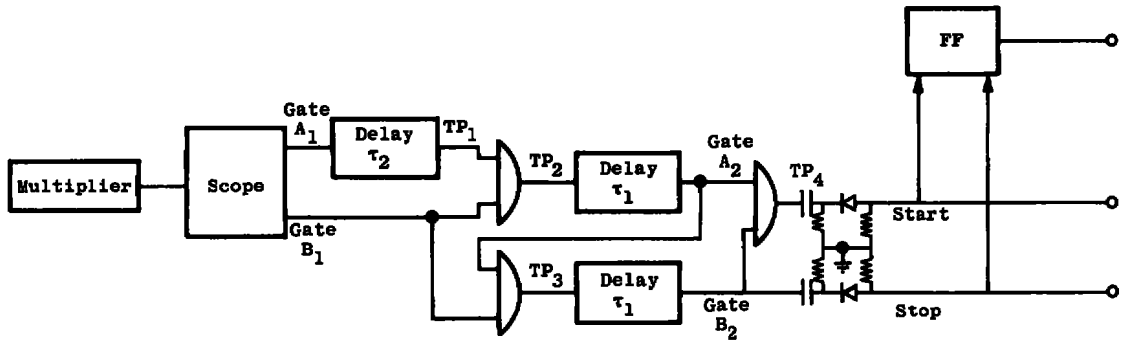

Fig. 22 Particle Velocity Instrumentation Schematic

For average velocity measurements, the start pulse is used to turn on a counter and the stop pulse to turn off the counter. These functions, in essence, gate a 1-MHz counter oscillator of the same interval as the pulse width output. A second counter can be used to count the number of times that a doublet is detected. The quotient of the total count and doublet count is a measure of the mean flight time in microseconds.

The use of more complicated data handling equipment for recording and counting the number of particles in a given velocity interval could provide a system which would yield a velocity distribution for the particles; however, further refinement of the system was discontinued after it became evident that the particles could not be accelerated to the free-stream gas velocity by drag forces, thus making useless the data taken in any particle collection efficiency tests using these low-speed particles. An analysis of the particle acceleration is given in the Appendix.

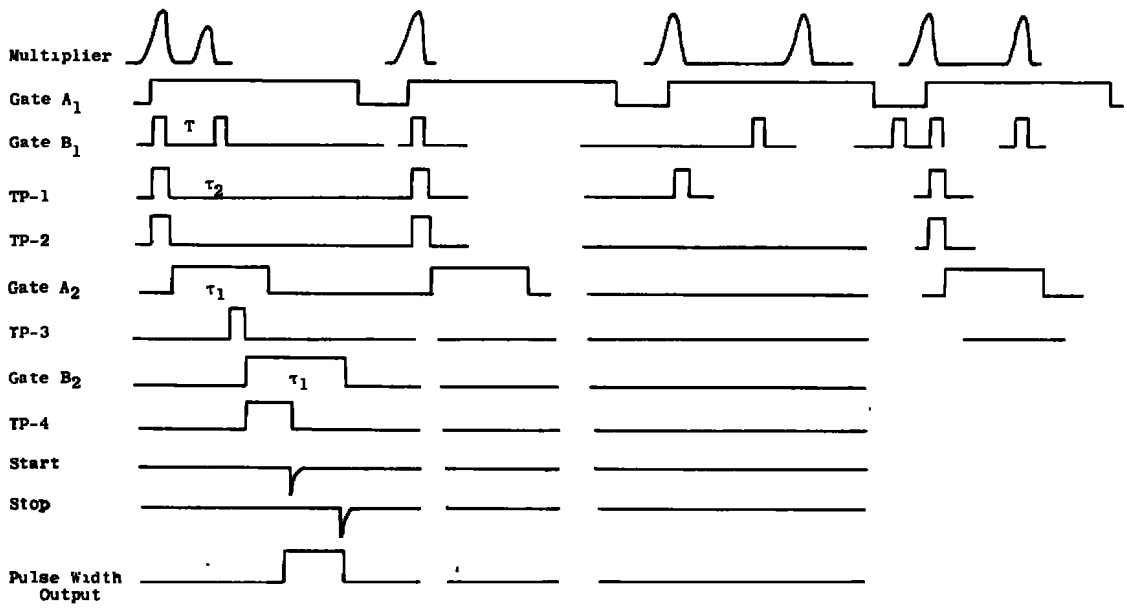

Fig. 23 Particle Velocity Gating Diagram

SECTION VII
CONCLUSIONS

In conclusion, the following have been demonstrated by the tests on the ALARR payloads:

1. At Mach number 2 flow conditions at altitudes ranging from 160,000 to 190,000 ft, the spiked AFIT payload did not operate satisfactorily because of the boundary-layer build-up in the throat of the spiked inlet.
2. At Mach numbers from 2 to 3 and at altitudes from 160,000 to 235,000 ft, the unspiked inlet AFIT payload showed maximum pressure recovery.
3. At Mach numbers 2 and 3, for altitudes from 160,000 to 235,000 ft, Varian Configuration 1 swallowed the normal shock in from 10 to 50 sec. Above 235,000 ft, flow becomes so rarefied and viscous that the shock could not be swallowed.
4. Varian Configuration 2, for the same altitude conditions, did not swallow the normal shock because of the large pressure drop produced by the filter paper normal to the flow.

5. At 10-deg angle of attack, the payloads did not show a significant loss in total pressure.

6. The micron-sized particles which were generated in Mach number 3.5 low density flow could not be accelerated to the free-stream gas velocity because of the rarefaction of the gas. The laser technique indicated that the particle velocity was about 100 ft/sec.

REFERENCES

1. "A Study of the Filtration and Permeability Characteristics of IPC 1478 Filter Paper." NASA Report No. 69, Institute of Paper Chemistry, 1960.

2. Collins, J. A., Jr. "Performance of an Air Sampling Probe in Mach 3.1 and Mach 1.9 Low Density Airstreams." AEDC-TR-65-20 (AD455961), January 1965.

3. Schaaf, S. A. and Cambré, P. L. "Flow of Rarefied Gases," Fundamentals of Gas Dynamics. Edited by H. W. Emmons. Princeton Series, Vol. III, Princeton, New Jersey, 1958.

APPENDIX
THEORETICAL DETERMINATION OF PARTICLE VELOCITIES IN LOW DENSITY FLOW

INTRODUCTION

Drag is the main force accelerating (decelerating) the particles in fluid flow and is given by the following equation.

$$D = m_p \ddot{x}_p = C_D \rho_g (u_g - u_p)^2 \pi \frac{d_p^2}{8} \tag{1}$$

Two values for the coefficient of drag were used in this analysis. For molecular speed ratios greater than 2, the coefficient of drag was assumed to be equal to 3. For molecular speed ratios less than 2, the coefficient of drag was assumed to be that of a sphere in free-molecular flow having only specular reflection (Ref. 3).

$$C_D = \frac{4S^4 + S^2 - 1}{2S^2} \operatorname{erf}(S) + \frac{e - \frac{S^2}{2}}{\sqrt{\pi S^3}} (1 + 2S^2)$$

ACCELERATION OF PARTICLES IN MACH NUMBER 3 NOZZLE

The Mach number 3 nozzle used is a conical nozzle with a 27-cm-diam throat and a length of 140 cm. The gas velocity 30 cm ahead of the nozzle throat was assumed to be zero.

$$D = m_p \frac{du_p}{dt} \tag{2}$$

Rewriting $\frac{du_p}{dt}$ as $\frac{du_p}{dX} \cdot \frac{dX}{dt} = u_p \frac{d(u_p)}{dX}$ (3)

and letting

$$D = C_D \rho_g \frac{\pi}{8} d_p^2 u^2$$

where

$$u = u_g - u_p$$

Eq. (2) becomes

$$u_p \frac{du_p}{dX} = \frac{\pi}{8} \frac{C_D d_p^2 \rho_g}{m_p} (u_g - u_p)^2 \tag{4}$$

with $m_p = \rho_p \frac{\pi d_p^3}{6}$ and, from the continuity equation,

$$\rho_g = \frac{\rho^* u^*}{(A/A^*) u_g}$$

and

$$\rho^* u^* = 0.578 \rho a_0 = 3.23 + 10^{-2} P_0$$

for air, Eq. (4) then becomes

$$u_g u_p \frac{du_p}{dX} = \frac{2.43 \times 10^{-2}}{(A/A^*)} \frac{C_D - P_o}{\rho_p d_p} (u_g - u_p)^2 \tag{5}$$

or

$$u_g u_p \frac{du_p}{dX} = \frac{2.43 \times 10^{-2}}{(A/A^*)} \gamma (u_g - u_p)^2 \tag{6}$$

where

$$\gamma = \frac{C_D P_0}{\rho_p d_p}$$

Now, the average gas velocity and average gas density were calculated along the nozzle axis for intervals of 10 and 20 cm (Fig. I-1). For different P_p and d_p, the particle velocity distribution was obtained along the nozzle axis in step-by-step calculations using Eq. (6). Figure I-2 shows the particle velocity distribution for different γ. A curve of $\left(\frac{u_g - u_p}{u_g}\right)_{exit}$ versus γ is plotted in Fig. I-3.

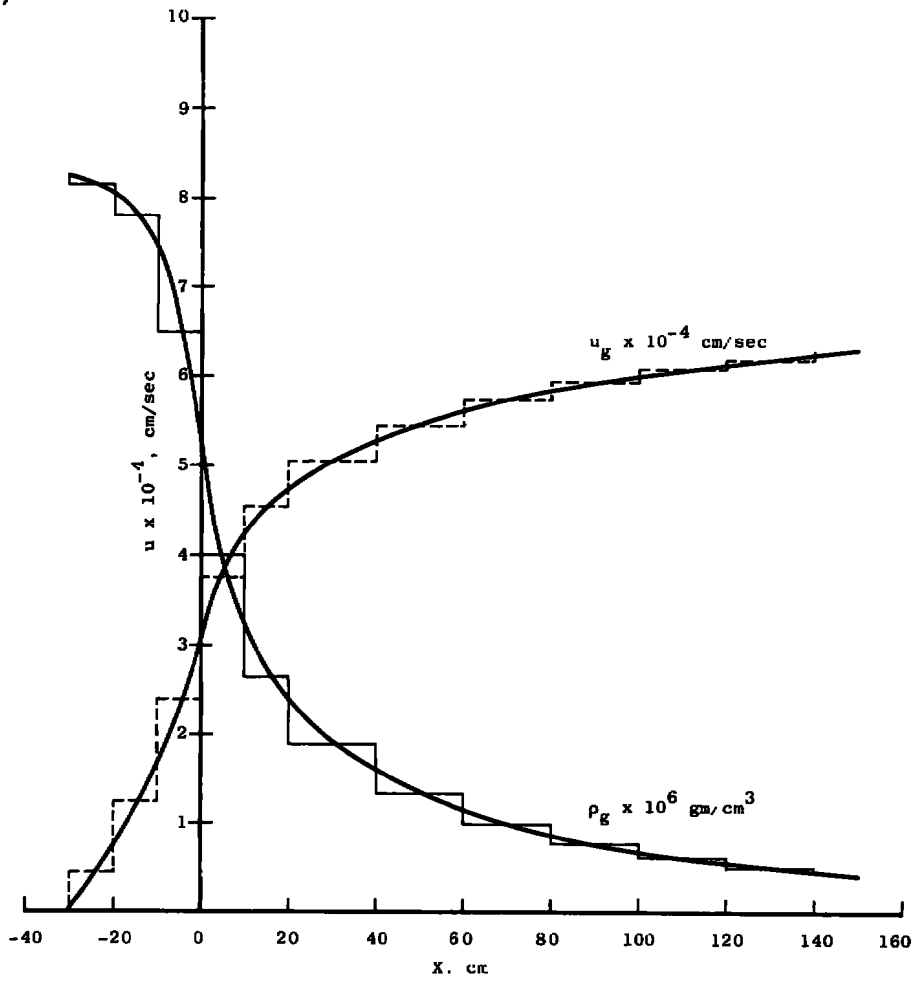

Fig. I-1 Gas Velocity and Gas Density Distribution along Nozzle Axis

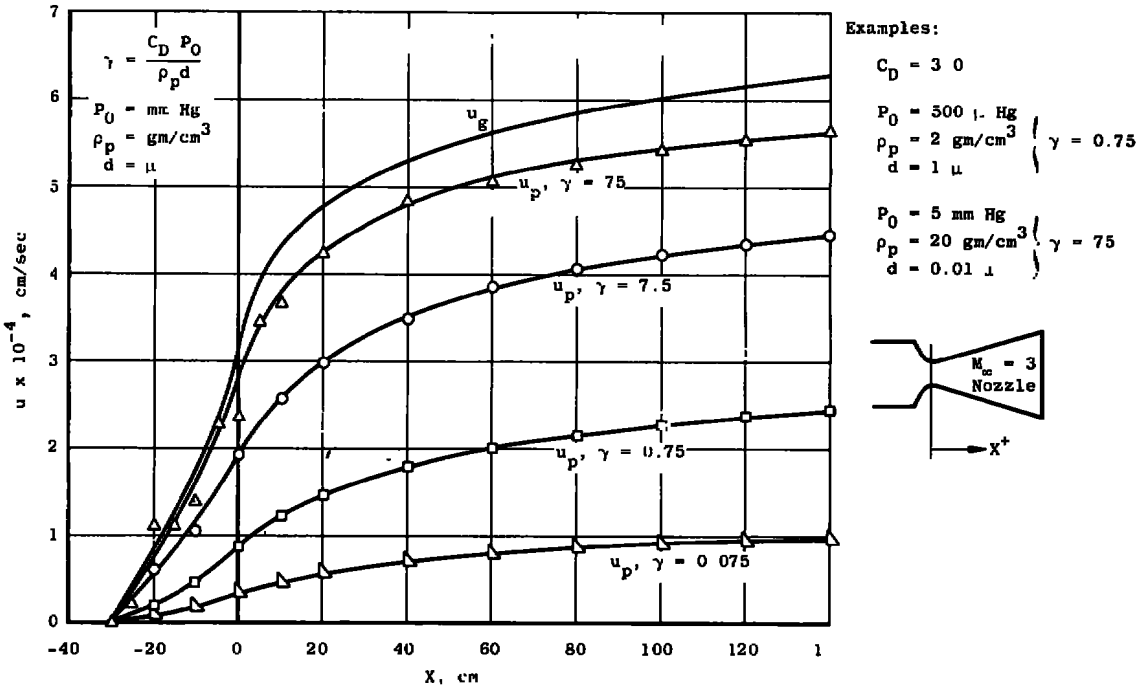

Fig. I-2 Particle Velocity Distribution for Different γ

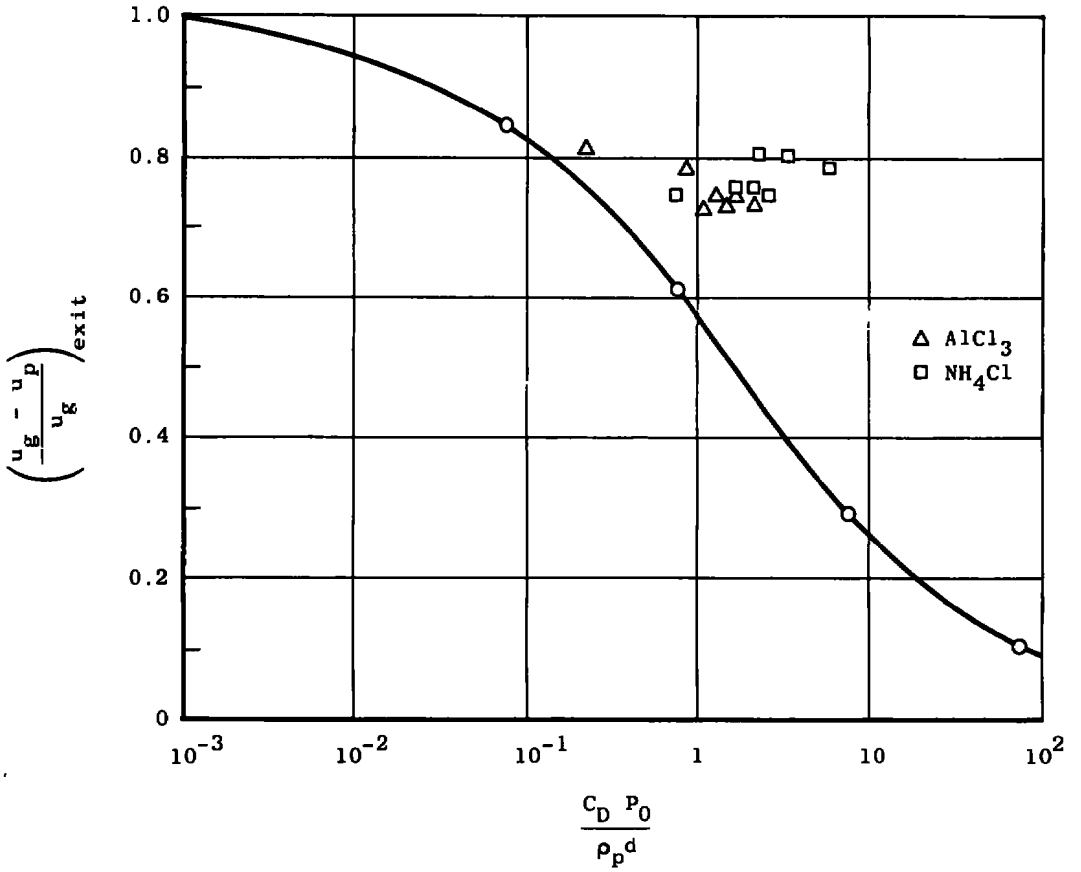

Fig. I-3 Exit Velocity Ratio versus γ

Particle velocities obtained experimentally at the nozzle exit are also plotted in Fig. I-3. The deviation between theory and experiment might be explained by the fact that there was no way of measuring the particle density, and the value used was the room temperature bulk density.

Calculations were also made assuming the gas velocity to be zero at 80, 40, and 10 cm ahead of the nozzle throat (Fig. I-4). The results show no appreciable change in the particle velocity at the nozzle exit.

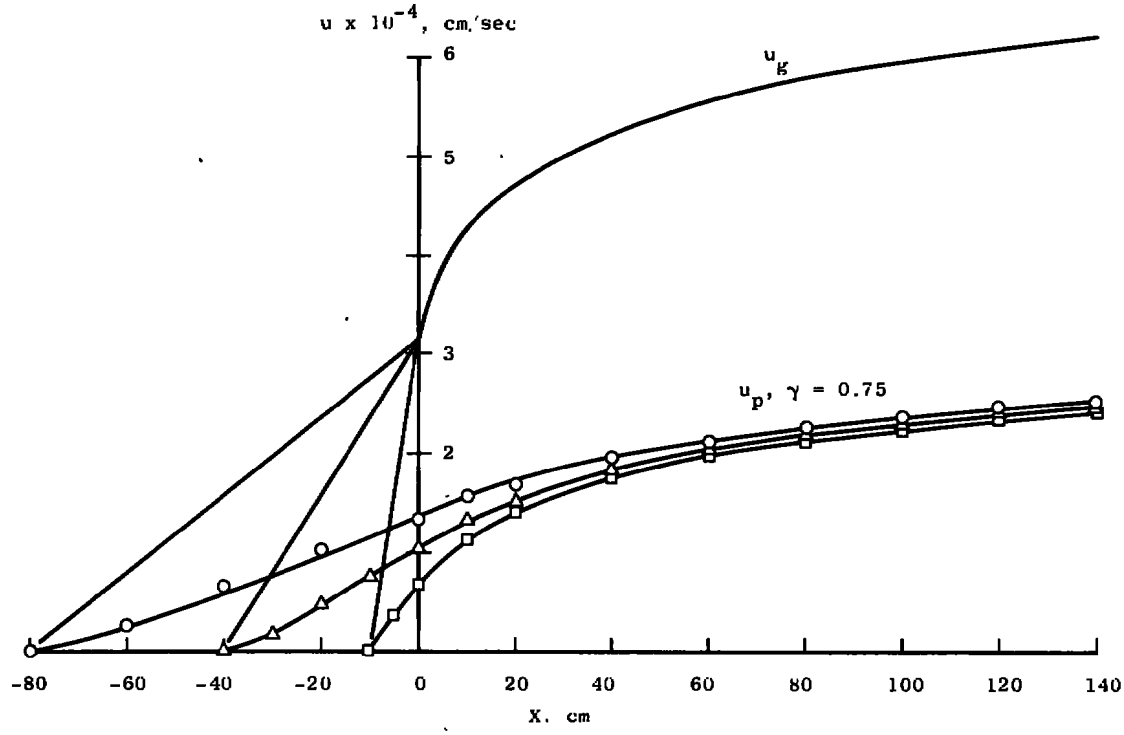

Fig. I-4 Particle Velocity Distribution for Different Contraction Section Lengths

Now, for free-molecular flow drag, let

$$C_D = \left(\frac{4S^4 + 4S^2 - 1}{2S^4}\right) \text{erf}\,(S) + \frac{e^{-\frac{S^2}{2}}}{S^3\sqrt{\pi}}\,(1 + 2S^2) \qquad (7)$$

where

$$e^{-\frac{S^2}{2}} = 1 - \frac{S^2}{2} + \frac{S^4}{8} - \frac{S^6}{48}$$

and

$$\text{erf}\,(S) = \frac{2S}{\sqrt{\pi}}\left(1 - \frac{S^2}{3} + \frac{S^4}{10} \ldots .\right)$$

For

$$S << 1, e^{-\frac{S^2}{2}} = 1 - \frac{S^2}{2}$$

and

$$\text{erf}\,(S) = \frac{2S}{\sqrt{\pi}}$$

Substitution into Eq. (7) yields

$$C_D = \frac{1}{\sqrt{\pi}} \left[3S = \frac{11}{2S}\right] \tag{8}$$

Using Eq. (4)

$$\frac{d(u_p^2)}{dX_p} = \frac{3}{2} \frac{C_D \rho_g u^2}{\rho_p d_p} \text{ where } u^2 = (u_g - u_p)^2$$

and

$$\rho_g u^2 = K_p m^2 = 2_p S^2$$

the final equation is

$$\frac{d(u_p^2)}{dX_p} = \frac{3_p}{\rho_p d_p \sqrt{\pi}} (3\,S^3 + \frac{11}{2} S) \tag{9}$$

For $S > 1$, C_D was obtained from Fig. 11 (Ref. 3). Figure I-5 is a plot of C_D versus S.

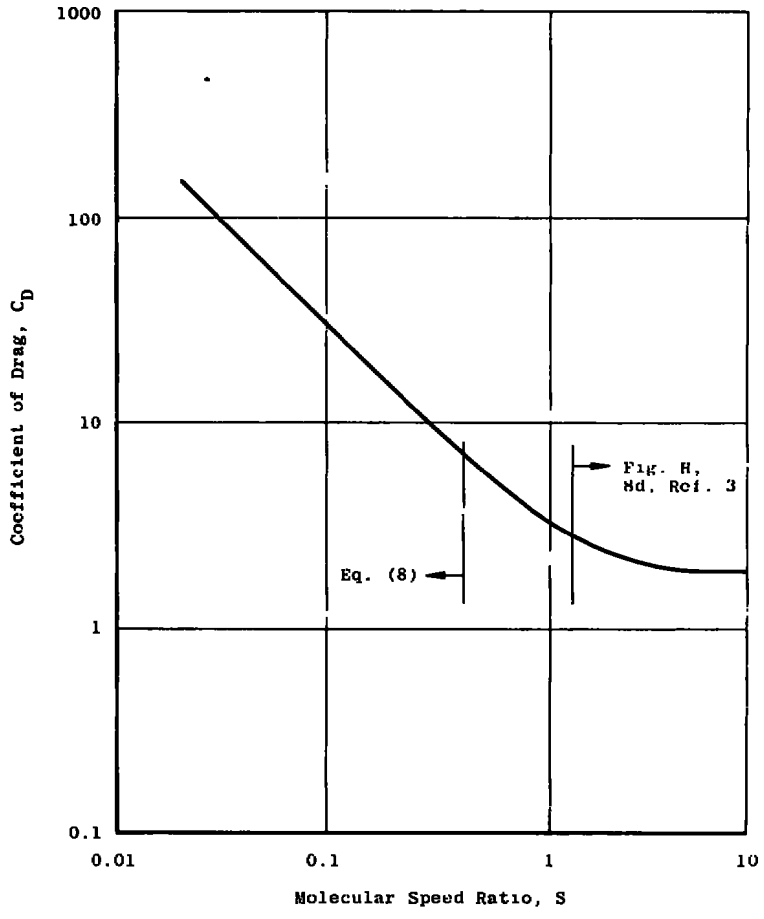

Fig. I-5 Free-Molecular Flow C_D for a Sphere (Specular Reflection Only)

The free-molecular flow particle velocity distribution is plotted in Fig. I-6, and the result is similar to that obtained when $C_D = 3$.

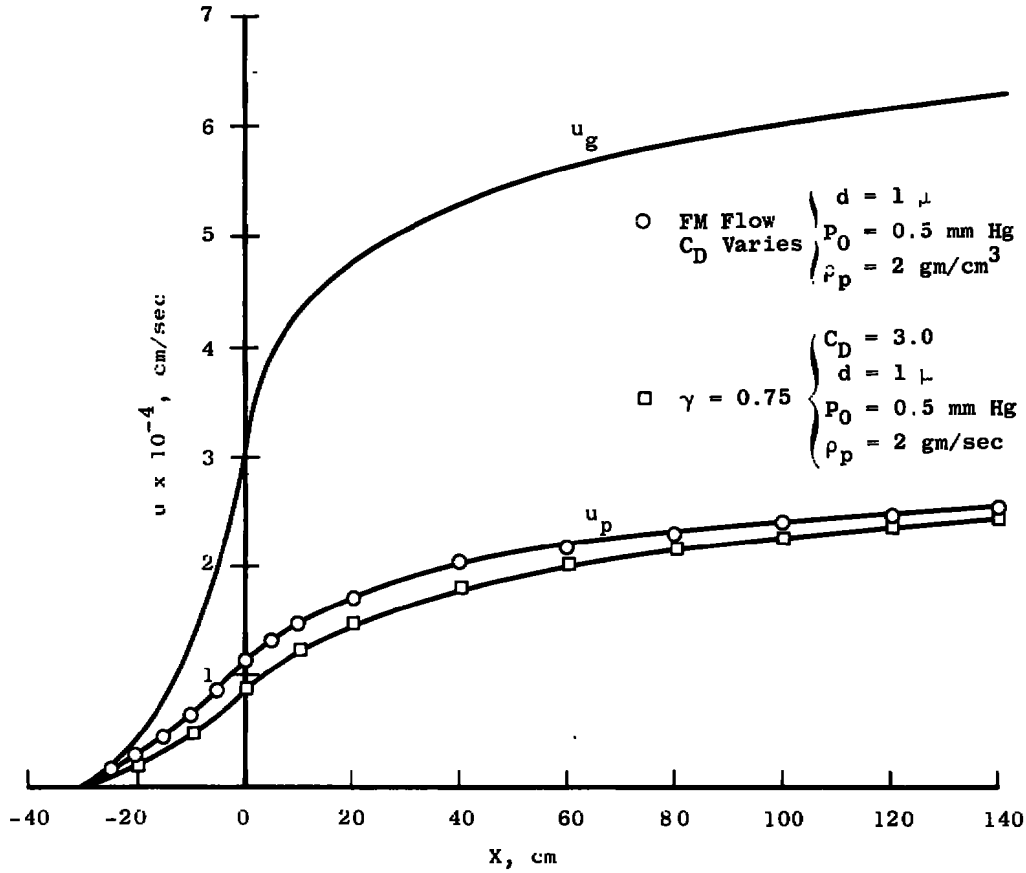

Fig. I-6 Particle Velocity Distribution for Varying C_D and C_D = Constant

DECELERATION OF PARTICLES IN A TUBE FILLED WITH AIR

The deceleration of particles within the collection probe is considered. For simplification, the probe is taken to be a tube filled with still air. It is assumed that the particles are not decelerated through the shock itself.

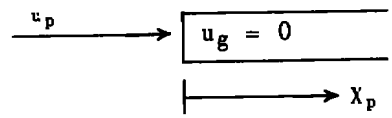

Now substituting $m_p = \rho_p \frac{\pi}{6} d_p^3$ and $\ddot{x}_p = u_p \frac{d(u_p)}{dX_p}$ into Eq. (1) gives

$$\frac{d(u_p)}{dX_p} = -\frac{3}{4} \frac{C_D \rho_g u_p}{\rho_p d_p}$$

For C_D = constant

$$\ell n\, u_p = -\frac{3}{4} \frac{C_D \rho_g}{\rho_p d_p} X_p + C_1$$

at $X = 0$, $u_p = u_i$

yielding

$$\frac{u_p}{u_i} = e^{-\frac{3}{4}\frac{C_D \rho_g}{\rho_p d_p} X_p} \tag{10}$$

Since $S < 1$, or $M < 1.2$ is satisfied, from Fig. I-5 $C_D = \frac{3.2}{S}$

and Eq. (4) may be written as

$$2u_p \frac{du_p}{dX_p} = -\frac{3pS^2}{\rho_p d_p} \frac{3.2}{S}$$

where

$$S = \frac{u_p}{a}\sqrt{\frac{K}{2}} \quad , \quad P = \rho_g \frac{a^2}{K}, \text{ and } K = 1.4$$

and

$$\frac{du_p}{dX_p} = -\frac{4.8}{\sqrt{2K}} \frac{\rho a}{\rho_p d_p} = -\frac{2.87}{\rho_p d_p} \rho_g a$$

At $X_p = 0$, $u_p = u_i$

and

$$\frac{u_p}{u_i} = 1 - 2.87 \frac{\rho_g X_p}{\rho_p d_p} \frac{a}{u_i}$$

Now

$$\frac{u_i}{a_{local}} \approx 1.83 \qquad (M_\infty = 3.0)$$

and

$$\frac{u_p}{u_i} = 1 - 1.57 \frac{\rho_g X_p}{\rho_p d_p} \tag{11}$$

Equation (10), with $C_D = 3$, and Eq. (11) are plotted in Fig. I-7. For values of $\frac{u_p}{u_i} \geq 0.5$ there is no significant difference between the two curves, and it is concluded that the particle deceleration from drag within the sampling probe is insufficient to prevent the particles which enter the probe from traversing the length of the probe and reaching the collection surfaces. That is, for $\frac{u_p}{u_i} \geq 0.5$, the capture performance of the sampling probe is unaffected by drag within the probe.

From Eq. (11), when $\frac{u_p}{u_i} \geq 0.5$, $1.57 \frac{\rho_g X_p}{\rho_p d_p} \leq 0.5$. Noting that Eq. (11) is conservative in that it assumes that u_g within the probe is zero when actually $u_g > 0$, and assuming $d_p = 10^{-4}$ cm, $\rho_p = 2$ g/cm^3, and $X_p = 50$ cm, the inequality indicates $\rho_g \leq 1.2 \times 10^{-6}$ g/cm^3. For free-stream conditions, $\rho_\infty = \frac{\rho_0}{4.31} = 2.79 \times 10^{-7}$ g/cm^3, corresponding to approximately 60-km altitude. Hence, for altitudes greater than 60 km (197,000 ft), the probe collection loss of ingested particles will be negligible.

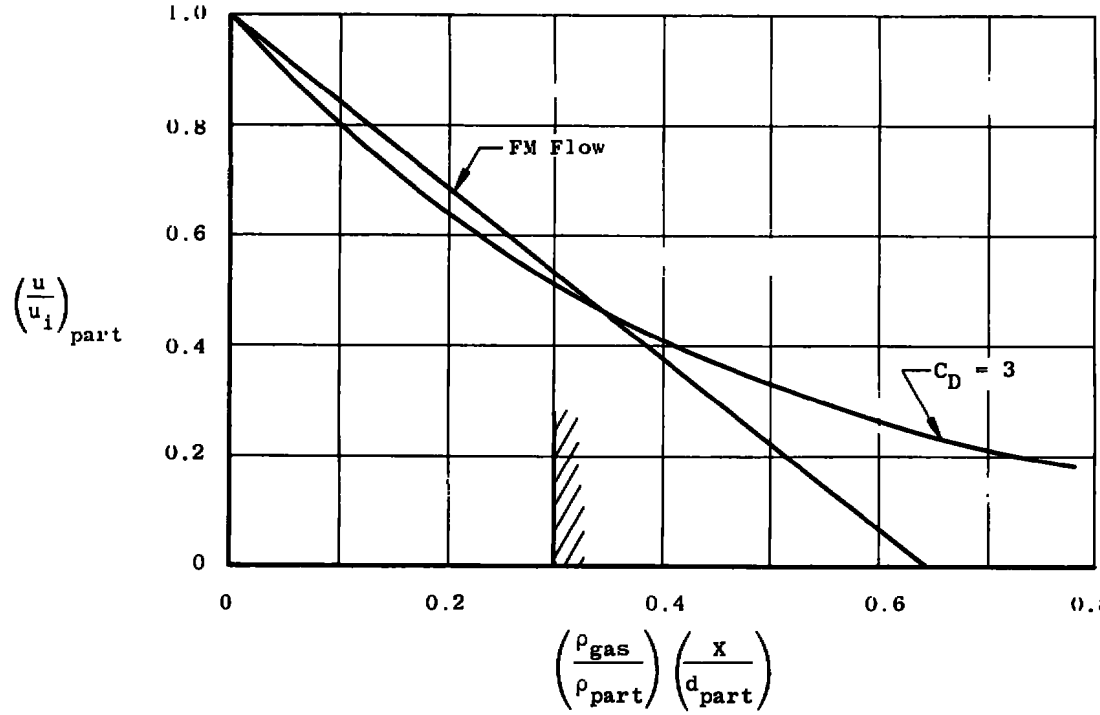

Fig. I-7 Particle Deceleration in a Tube Filled with Air

FIRST APPROXIMATION OF PARTICLE LOSS BETWEEN BOW SHOCK AND INTAKE

The loss of particles caused by flow spillage at the probe inlet (shock detached) is considered. The aerodynamic efficiency is $\eta_{aero} = \left(\frac{d_\infty}{D}\right)^2$, and the particle efficiency η_p is always $\geq \eta_{aero}$. Taking the most severe case, let $\eta_{aero} < 0$.

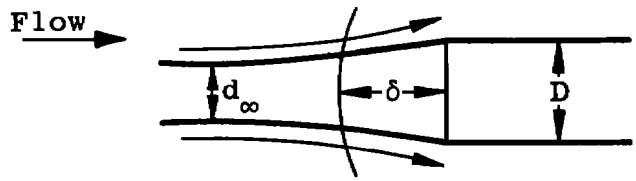

The maximum residence time of a particle between the shock and the inlet δ is $\Delta t_{max} < \frac{2\delta}{u_2} + \frac{D}{u_2^*}$ where $\frac{\delta}{u_2/2}$ is the time it takes for the particle to linearly decelerate from u_2 to u = 0 in the X-direction, and $\frac{D/2}{u_2^*/2}$ is the time it takes for the linear acceleration of the particle in the Y-direction (from u = 0 to u_2^*), assuming sonic velocity at the corner.

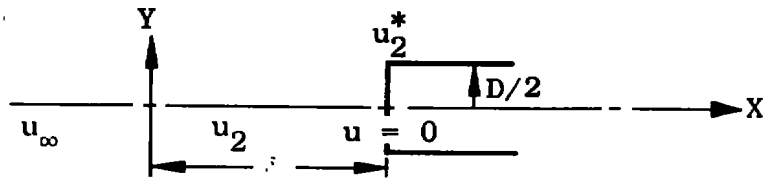

The minimum residence time of a particle in the shock layer is $\Delta t_{min} = \frac{\delta}{u_\infty}$ when the particle is not decelerated at all in X-direction. For M = 3 and $\delta/D = 0.4$,

$$\frac{(\Delta t_{max})}{(\Delta t_{min})} = 12.3$$

Assuming free-molecular flow and since S < 1 behind the normal shock, the drag force (Eq. (1)) becomes

$$D = \rho_p \frac{\pi}{6} d_p^3 \ddot{x}_p = \frac{\pi}{4} d_p^2 \; P \; S^2 \; \frac{3.2}{S}$$

where

$$S = 0.837 \frac{u_2}{a_2} \text{ and } P \approx P_0'$$

giving

$$D = 2.10 \frac{P_0' \, d_p^2}{a_2} u_2$$

The maximum force acting in the Y-direction is

$$m\ddot{Y} = D_{max} = 2.10 \frac{P_0' \, d_p^2}{a_2} u_2^*$$

Assuming that the force $D_{max}/2$ works on the particle for a period of $5(\Delta t)_{min}$ (a conservative estimate) yields

$$Y_{max} = \frac{1}{2} \left(\frac{D_{max}}{2}\right) 25 \frac{(\Delta t)^2}{m} \text{ or } Y_{max} = 25.2 \frac{u_2^*}{a_2} \frac{P_0'}{\rho_p \, d_p} \left(\frac{\delta}{u_\infty}\right)^2 \qquad (12)$$

When $\eta_p > 0.95$, $\frac{Y_{max}}{D}$ will be < 0.0125, and less than 5 percent of the particles will be lost to the probe from spillage between the bow shock and the sampling probe inlet. Hence,

$$\frac{Y_{max}}{D} = 25.2 \frac{u_2^*}{a_2} \frac{P_0'}{\rho_p \, d_p} \left(\frac{\delta}{u_\rho}\right)^2 \frac{1}{D} \leq 0.0125$$

or

$$P_0' \leq \frac{0.0125}{25.2} \left(\frac{a_2}{u_2^*}\right)\left(\frac{u_\rho}{\delta}\right)^2 \rho_p \, d_p \, D$$

Letting

$$D = 15 \text{ cm}, \delta = 0.4D = 6 \text{ cm}, u_\infty = 9.0 \times 10^4 \text{ cm/sec}, d_p = 10^{-4} \text{ cm}, \rho_p = 2 \text{ g/cm}^3$$

and $\frac{u^*_2}{a^2} \approx 1$,

$$P'_0 \leq 3.35 \times 10^2 \text{ dyne/cm}^2$$

P_∞ is then ≤ 0.0209 mm Hg, corresponding to an altitude of 74 km. Hence, for altitudes in excess of approximately 74 km (243,000 ft), the particles lost to the probe from spillage between the bow shock and the sampling probe inlet will be negligible.

UNCLASSIFIED

Security Classification

DOCUMENT CONTROL DATA - R & D

(Security classification of title, body of abstract and indexing annotation must be entered when the overall report is classified)

1 ORIGINATING ACTIVITY (Corporate author)	2a. REPORT SECURITY CLASSIFICATION
Arnold Engineering Development Center ARO, Inc., Operating Contractor Arnold Air Force Station, Tennessee	UNCLASSIFIED
	2b. GROUP N/A

3 REPORT TITLE

INVESTIGATION OF TWO TYPES OF ALARR HIGH ALTITUDE AIR SAMPLING PROBES IN SUPERSONIC LOW DENSITY AIRSTREAMS (PROJECT VELA-SURFACE)

4 DESCRIPTIVE NOTES (Type of report and inclusive dates)

October 19, 1966 to October 25, 1967 - Final Report

5. AUTHOR(S) (First name, middle initial, last name)

D. W. Hill, C. E. Pinion, and D. K. Smith, ARO, Inc.

6 REPORT DATE	7a. TOTAL NO. OF PAGES	7b. NO OF REFS
April 1969	43	3

8a. CONTRACT OR GRANT NO.	9a. ORIGINATOR'S REPORT NUMBER(S)
F40600-69-C-0001	
b. PROJECT NO 9087	AEDC-TR-69-4
c. System 921A	9b. OTHER REPORT NO(S) (Any other numbers that may be assigned this report)
d.	N/A

10 DISTRIBUTION STATEMENT This document is subject to special export controls and each transmittal to foreign governments or foreign nationals may be made only with prior approval of Air Force Tactical Air Command (TD-6D), Alexandria, Virginia 22310.

11 SUPPLEMENTARY NOTES	12. SPONSORING MILITARY ACTIVITY
Available in DDC.	Air Force Tactical Air Command (TD-6D), Alexandria, Virginia 22310

13 ABSTRACT

Experimental investigations were made to determine aerodynamic performance of high altitude air sampling probes. Three flowthrough-type probes and a probe with a liquid-nitrogen-cooled charcoal pump were tested at pressure altitudes from 160,000 to 260,000 ft in airflows ranging from Mach number 1.8 to 3.5. The investigations indicate that the boundary layer begins to merge in the flowthrough-type supersonic diffusers below a Reynolds number per foot of 2×10^4. The charcoal pump probe indicated that there is a 0.2- to 5.0-scf transition in pumping between Reynolds numbers per foot of 1.5×10^2 and 1.4×10^4. Further investigations were made to determine the velocity attained by micron-sized particles which were generated in Mach number 3.5 low density airstreams. The results indicate the gas density was too rarefied to accelerate the particles to the free-stream velocity.

This document is subject to special export controls and each transmittal to foreign governments or foreign nationals may be made only with prior approval of Air Force Tactical Air Command (TD-6D), Alexandria, Virginia 22310.

This document has been approved for public release and sale; its distribution is unlimited. PenTAB 72-19, D+D 10 Oct, 72.

DD FORM 1 NOV 65 1473

UNCLASSIFIED

Security Classification

14 KEY WORDS	LINK A		LINK B		LINK C	
	ROLE	WT	ROLE	WT	ROLE	WT
1, Air Launch Air Recovery Rocket						
2 probes						
3 sampling						
altitude simulation						
performance						
low density						
supersonic flow						
4 Project VELA-SURFACE						
5. air .. sampling .						
1 - 2 ,						